Development 140, 3028-3039 (2013) doi:10.1242/dev.094839

Gpr125 modulates Dishevelled distribution and planar cell polarity signaling

Xin Li[1,2], Isabelle Roszko[3], Diane S. Sepich[3], Mingwei Ni[4], Heidi E. Hamm[1,5], Florence L. Marlow[2,*] and Lilianna Solnica-Krezel[1,3,6,*]

SUMMARY

During vertebrate gastrulation, Wnt/planar cell polarity (PCP) signaling orchestrates polarized cell behaviors underlying convergence and extension (C&E) movements to narrow embryonic tissues mediolaterally and lengthen them anteroposteriorly. Here, we have identified Gpr125, an adhesion G protein-coupled receptor, as a novel modulator of the Wnt/PCP signaling system. Excess Gpr125 impaired C&E movements and the underlying cell and molecular polarities. Reduced Gpr125 function exacerbated the C&E and facial branchiomotor neuron (FBMN) migration defects of embryos with reduced Wnt/PCP signaling. At the molecular level, Gpr125 recruited Dishevelled to the cell membrane, a prerequisite for Wnt/PCP activation. Moreover, Gpr125 and Dvl mutually clustered one another to form discrete membrane subdomains, and the Gpr125 intracellular domain directly interacted with Dvl in pull-down assays. Intriguingly, Dvl and Gpr125 were able to recruit a subset of PCP components into membrane subdomains, suggesting that Gpr125 may modulate the composition of Wnt/PCP membrane complexes. Our study reveals a role for Gpr125 in PCP-mediated processes and provides mechanistic insight into Wnt/PCP signaling.

KEY WORDS: Gastrulation movements, Convergence and extension, Facial branchiomotor neuron, Zebrafish

INTRODUCTION

During embryogenesis, gastrulation establishes the three germ layers and the animal body plan. Vertebrate gastrulation relies on polarized cell behaviors to drive convergence and extension (C&E) movements that narrow embryonic tissues mediolaterally and elongate them anteroposteriorly (Keller et al., 2000; Solnica-Krezel, 2005; Yin et al., 2009; Gray et al., 2011). In dorsal regions of *Xenopus* and zebrafish gastrulae, cells become elongated and align along the mediolateral embryonic axis, allowing preferential intercalation between their anterior and posterior neighbors to drive C&E (Keller et al., 2000; Topczewski et al., 2001; Jessen et al., 2002; Marlow et al., 2002; Lin et al., 2005). Modulation of cell adhesion and intercellular signaling have been proposed to instruct such complex cell behaviors (Yin et al., 2009). However, the molecules implementing these actions have not been fully identified.

Currently, the Wnt/PCP signaling system, which is equivalent to the PCP pathway coordinating wing hair and ommatidia orientation in *Drosophila* (Simons and Mlodzik, 2008; Goodrich and Strutt, 2011), is the best-studied pathway regulating C&E movements in vertebrates (Tada and Kai, 2009; Yin et al., 2009; Gray et al., 2011). Polarized cell behaviors that underlie C&E, including directed cell migration and polarized planar and radial intercalations, are exquisitely sensitive to PCP signaling levels, as excess or insufficient Wnt/PCP pathway component function impairs C&E movements (Wallingford et al., 2000; Jessen et al., 2002; Marlow et al., 2002; Carreira-Barbosa et al., 2003). In addition to regulating C&E, a subset of Wnt/PCP components also regulates the caudal tangential migration of facial branchiomotor neurons (FBMN) in zebrafish and mouse (Jessen et al., 2002; Carreira-Barbosa et al., 2003; Wada et al., 2005; Wada et al., 2006; Wada and Okamoto, 2009).

PCP pathway components are known to localize asymmetrically in multiple tissues that manifest planar polarity. In the fly wing epithelia, the receptor Frizzled and cytoplasmic proteins Dishevelled (Dsh/Dvl in vertebrates) and Diego localize to the distal side of the cell, where the wing hair will eventually emerge. By contrast, the transmembrane protein Van gogh/Strabismus and cytoplasmic protein Prickle (Pk) localize proximally, whereas the seven transmembrane protocadherin Flamingo/Starry night is present at both cell edges (Axelrod, 2001; Feiguin et al., 2001; Strutt et al., 2002; Tree et al., 2002; Bastock et al., 2003). This stereotyped asymmetric localization of Pk and Dvl on opposing anterior and posterior membranes has been observed in the neural plate and dorsal mesodermal cells undergoing C&E in zebrafish (Ciruna et al., 2006; Yin et al., 2008). Such molecular asymmetries are considered to be either a consequence of cell polarization or an essential step in the process of Wnt/PCP-mediated cell polarization (Simons and Mlodzik, 2008; McNeill, 2010; Goodrich and Strutt, 2011; Gray et al., 2011).

Asymmetric localization of PCP components in polarized epithelia and protein interaction studies supports a model whereby PCP components interact in asymmetric membrane complexes spanning the juxtaposed cells to generate planar polarization (McNeill, 2010; Goodrich and Strutt, 2011). Recently, Dsh was shown to cluster PCP complexes into membrane subdomains in cells of *Drosophila* pupal wings (Strutt et al., 2011), raising the possibility that clustering of asymmetric PCP complexes into membrane subdomains might provide a local self-enhancement mechanism that establishes and/or maintains planar polarity (Strutt

[1]Neuroscience Graduate Program, Vanderbilt University School of Medicine, Nashville, TN 37232, USA. [2]Department of Developmental and Molecular Biology, Albert Einstein College of Medicine, Bronx, NY 10461, USA. [3]Department of Developmental Biology, Washington University School of Medicine, St Louis, MO 63110, USA. [4]Department of Surgery, New York Hospital Medical Center of Queens, Flushing, NY 11355, USA. [5]Department of Pharmacology, Vanderbilt University School of Medicine, Nashville, TN 37232, USA. [6]Department of Biological Sciences, Vanderbilt University, Nashville, TN 37232, USA.

*Authors for correspondence (florence.marlow@einstein.yu.edu; solnical@wustl.edu)

Accepted 2 May 2013

et al., 2011). Interestingly, membrane clustering of PCP components occurs between *Xenopus* Van gogh-like 2 (Vangl2, vertebrate homolog of Van gogh/Strabismus) and *Drosophila* Pk expressed in *Xenopus* animal cap explants, and among zebrafish Frizzled7 (Fzd7), Wnt11 and *Xenopus* Dvl expressed in zebrafish blastula (Jenny et al., 2003; Witzel et al., 2006). In the latter case, subdomain formation correlates with increased persistence of membrane contacts partially dependent on vertebrate Flamingo homologues, Cadherin EGF LAG seven-pass G-type receptors (Celsrs) (Witzel et al., 2006).

Celsrs belong to the family of adhesion G protein-coupled receptors (GPCRs), which are chimeras of adhesion molecules and transmembrane signal transducer GPCRs (Fredriksson et al., 2003). Owing to their unique structure, adhesion GPCRs are postulated to play dual roles in cell adhesion and signal transduction (Yona et al., 2008). Recent studies of GPR56, GPR124 and Gpr126 implicate adhesion GPCRs in diverse developmental processes, including brain development, blood vessel formation and myelination in zebrafish and mammals (Kuhnert et al., 2010; Piao et al., 2004; Monk et al., 2009; Monk et al., 2011). As components of the PCP pathway, Celsr adhesion GPCRs have been reported to regulate zebrafish gastrulation and FBMN migration (Formstone and Mason, 2005; Wada et al., 2006; Carreira-Barbosa et al., 2009).

To better understand the molecular mechanisms underlying gastrulation movements and to uncover the functions of uncharacterized adhesion GPCRs, we surveyed adhesion GPCRs for candidate regulators of zebrafish gastrulation. Here, we have identified Gpr125 adhesion GPCR as a modulator of C&E gastrulation movements and FBMN migration. Gpr125 functionally interacts with multiple Wnt/PCP components and directly interacts via its intracellular domain with Dvl. Mutual redistribution of Gpr125 and Dvl fusion proteins into discrete membrane subdomains and their ability to selectively recruit additional PCP components into these domains suggest that Gpr125 might act as a component of the PCP membrane complexes and modulator of Wnt/PCP signaling in vertebrates.

MATERIALS AND METHODS

Zebrafish lines

AB, ABWIK, *llk*^{RW468}, *tri*^{vu67} (a nonsense allele; Chunyue Yin, Jason R. Jessen, I.R. and L.S.K., unpublished), *slb*^{tz216}, *tp53*^{M214K} and Tg(*isl1:GFP*) were used in this study (Heisenberg et al., 2000; Jessen et al., 2002; Berghmans et al., 2005; Wada et al., 2005). Embryos obtained from natural spawnings were staged according to morphological criteria (Kimmel et al., 1995).

RT-PCR and cloning of zebrafish *gpr125*

Total RNA was extracted with TRI$_{ZOL}$ LS reagent (Invitrogen) from wild-type embryos at the indicated stages. cDNA was produced with SuperScript III first-strand synthesis system (Invitrogen). To detect *gpr125* transcripts, PCR was performed using *gpr125*-q primers (supplementary material Table S1) with GoTaq Flexi DNA polymerase (Promega). The full-length *gpr125*-coding sequence (GenBank Accession Number KC996731) was amplified using *gpr125*-fl primers (supplementary material Table S1) with Easy-A high-fidelity PCR cloning enzyme (Agilent Technologies) and subcloned into pCR8 vector (Invitrogen), from which various deletion forms of Gpr125 were amplified with the primers listed in supplementary material Table S1 and subcloned into pCR8 and subsequently into pCS-based vectors (Villefranc et al., 2007) or *E. coli* expression vector pDEST 15 (Invitrogen) with Gateway LR clonase II enzyme mix or LR clonase II plus enzyme (Invitrogen).

RNA and antisense morpholino oligonucleotide (MO) injection

Capped RNA was synthesized using mMessage mMachine Kit (Ambion). Two non-overlapping MOs (MO1-*gpr125* and MO2-*gpr125*) targeting the 5′UTR region were used. The effectiveness of each MO in blocking the translation of RNA encoding GFP fused to the MO target sequence (GFP reporter) was determined. The non-specific toxicity of MO1-*gpr125* was confirmed by complete suppression of cell death in *p53*$^{M214K/M214K}$ null mutants (supplementary material Fig. S2J,K). Sequences of all MOs used are listed in supplementary material Table S1.

Anteroposterior (AP) axis, notochord and somite measurements

Embryos were imaged using Olympus SZ61 or Zeiss Discovery dissecting microscopes and Olympus or Zeiss AxioCam MRM cameras in PictureFrame or Axiovision Rel 4.6 (Zeiss). For AP axis length, embryos were traced from the forebrain to the tip of the tail fin. For notochord width, straight lines were drawn perpendicular to the AP axis between the lateral borders of the notochord at level of first somites. For somite length, the first somites were traced. The distance was measured with ImageJ software (NIH) (Marlow et al., 1998).

Whole-mount *in situ* hybridization

Antisense probes were synthesized with RNA labeling kits (Roche). DNA fragments amplified with *gpr125*-probe1 primers and *gpr125*-probe2 primers (supplementary material Table S1) were used as templates for *gpr125* probe synthesis. Whole-mount *in situ* hybridization analyses were performed as described previously (Marlow et al., 1998).

Whole-mount immunostaining

Embryos were fixed in 100% Prefer fixative (Anatech) for 40 minutes at room temperature. Immunostaining was performed with a standard protocol. Antibodies were diluted in blocking buffer containing 0.5% BSA, 10% serum, 0.1% Triton X-100 and 2% DMSO in PBS. Primary antibodies used were: anti-zebrafish Tri/Vangl2 (rabbit, 1:500, made by the Vanderbilt University Antibody Core), anti-GFP (mouse, 1:500, Clontech, #632375) and rat anti-RFP (1:1000, Chromotek, clone 5F8). Secondary antibodies were: Alexa Fluor 568 goat anti-rat, Alexa Fluor 647 goat anti-rabbit and Alexa Fluor 488 goat anti-mouse (1:500, Invitrogen).

Cell polarity analyses

Measurements and analyses of length-width ratios (LWRs) and mediolateral alignment were performed according to Myers et al. (Myers et al., 2002). Wild-type embryos were injected with 200 pg *gpr125-Cherry* + 100 pg *membraneEGFP* (*mEGFP*), or 300 pg of *mEGFP* synthetic RNA. *membraneCherry* (*mCherry*) RNA (150 pg) was injected into *vangl2/tri* embryos for membrane labeling. Embryos were fixed overnight in 4% PFA and confocal stacks were collected. Image analysis was performed in ImageJ (NIH) and Fiji (Schindelin et al., 2012), where cells were outlined by hand. LWRs and angles of the long axis were measured with Fit Ellipse. Rose diagrams were drawn using Rose.NET (Todd A. Thompson; http://mypage.iu.edu/~tthomps/programs/home.htm).

In vivo subcellular protein localization analyses

Pk localization experiments: one-cell embryos were injected with 200 or 300 pg *gpr125* and 100 pg *mCherry* synthetic RNA, or an equivalent amount of *mCherry* RNA. At the 16-cell stage, one cell was injected with 16-19 pg of *pk-GFP* RNA (Yin et al., 2008). At tailbud to two-somite stage, *z*-stacks were collected using Quorum Spinning disc Confocal/ IX81-Olympus inverted microscope. Image analysis was performed in ImageJ (NIH) and Fiji.

To monitor protein localization in late blastulae, one-cell stage embryos were injected with specific combinations of RNA at doses specified in the figures. In mosaic expression experiments, *Histone2B-RFP* (*H2B-RFP*) and *gpr125FL* RNA were injected into one blastomere at the 16- to 32-cell stage. The superficial layer of live or immunostained blastulae at 4-5 hours post-fertilization (hpf) was imaged with a Zeiss Axioobserver Apotome fluorescence microscope equipped with a 40× oil lens (Zeiss) and MRm digital camera (Zeiss), and Axiovision Rel 4.7 software (Zeiss), Leica TCS SP5 confocal or Quorum Spinning disc Confocal/ IX81-Olympus inverted microscope and Metamorph Acquisition software. For Dvl-GFP subdomain quantification, embryos were imaged using identical settings for the green channel and cells from five embryos of each group were randomly selected for measuring membrane length, Dvl-GFP particle size and number in ImageJ

(NIH). The average threshold of three membranes expressing Dvl-GFP alone was used to set the background threshold for subdomain analysis. To monitor protein localization in the gastrulae, RNA were injected at the specified doses at the one-cell stage and embryos were fixed at 10 hpf for immunostaining. Images were acquired with a Quorum Spinning disc Confocal/IX81-Olympus inverted microscope and Metamorph Acquisition software.

Pull-down and western blot analyses

Control glutathione S-transferase (GST) protein was produced from pGEX-4T-1 (GE Healthcare) in XL-1Blue *E. coli* and GST-fusion proteins were produced from pDEST 15-based vectors in BL21-AI *E. coli* according to manufacturer's protocol (Invitrogen). Pierce glutathione magnetic beads (Thermo Scientific) were used in purification and subsequent pull-down experiments. Dvl-GFP and EGFP proteins were translated *in vitro* in TNT coupled reticulocyte lysate systems (Promega). Pull-down was performed according to the *Promega Protocols & Applications Guide* with the following modifications: cells were lysed in lysis buffer [50 mM NaH_2PO_4, 300 mM NaCl, 1 mM EDTA and 1% TritonX-100 (pH 8.0)] with freshly added Lysozyme (200 μg/ml), DTT (1 mM) and complete Mini EDTA-free protease inhibitor cocktail tablets, and washed in lysis buffer without lysozyme in the presence of 5% glycerol. All pull-down procedures were performed at 4°C. Denville Blue Protein Stain (Denville Scientific) was used to detect GST-fusion proteins in SDS-PAGE gels (Fisher Bioreagents). Western blot analysis was conducted with primary antibodies [mouse monoclonal anti-GFP antibody (1:2000, Roche, clones 7.1 and 13.1) and mouse monoclonal anti-GST antibody HRP conjugate (1:8000, Santa Cruz, sc-138HRP)] and a secondary antibody: goat polyclonal anti-mouse HRP conjugate (1:10,000, Millipore, 12-349). An Amersham ECL plus western blotting detection system (GE Healthcare) was used and signals were detected with Amersham Hyperfilm ECL (GE Healthcare) or Fujifilm LAS-3000.

Statistical analyses

Data analyses were performed in GraphPad Prism (GraphPad Software) and Excel (Microsoft). All results are expressed as mean±s.e.m. Differences between two groups were analyzed using a two-tailed Student's *t*-test. Differences among three groups were analyzed by one-way ANOVA, followed by Bonferroni's *post hoc* test. Statistical significance was set at $P<0.05$.

RESULTS

Excess Gpr125 disrupts C&E movements and underlying cell polarity

Like other adhesion GPCRs, Gpr125 has a long extracellular subunit with protein-protein interacting domains and a GPCR subunit (supplementary material Fig. S1A). The last four amino acids (ETTV) of Gpr125 constitute a PDZ-binding motif (supplementary material Fig. S1A), which is also found in the transmembrane PCP pathway components Frizzled and Vangl2 (Hering and Sheng, 2002; Jessen et al., 2002). Using semi-quantitative RT-PCR and whole-mount *in situ* hybridization analyses, we determined that *gpr125* transcripts were maternally provided and uniformly distributed at blastula and gastrula stages (supplementary material Fig. S1B-D). Notably, at 25 hpf, *gpr125* expression became enriched in the rostral region, including the hindbrain at the level of the otic vesicles, where tangential migration of FBMN occurs (supplementary material Fig. S1E) (Wada et al., 2005; Wada and Okamoto, 2009).

As gastrulation movements are sensitive to both elevated and reduced levels of their regulators (Wallingford et al., 2000; Jessen et al., 2002; Marlow et al., 2002; Carreira-Barbosa et al., 2003; Zeng et al., 2007; Lin et al., 2009), we investigated Gpr125 function through both gain- and loss-of-function approaches. Microinjection of synthetic *gpr125* RNA into wild-type zygotes caused dose-dependent shortening of the AP axis and synophthalmia or cyclopia (Fig. 1A-K), phenotypes suggestive of C&E defects (Marlow et al., 1998; Heisenberg et al., 2000; Topczewski et al., 2001; Jessen et al., 2002; Marlow et al., 2002; Carreira-Barbosa et al., 2003; Formstone and Mason, 2005). To determine whether such dysmorphologies were due to an earlier C&E gastrulation defect, we compared expression of tissue-specific markers in *gpr125* RNA-injected and control embryos at late gastrulation (two-somite stage) (Fig. 1L-O). The expression of *distal-less homeobox 3* (*dlx3*) in the border of the neural ectoderm, and *paraxial protocadherin* (*papc*) in the adaxial and paraxial mesoderm revealed mediolaterally broader but anteroposteriorly shorter neural ectoderm, notochord and somites (89%, $n=37$; Fig. 1M,O). In addition, the prechordal mesoderm, marked by *hatching gland 1* (*hgg1*), failed to migrate beyond the anterior edge of the neural ectoderm and was abnormally elongated in 35% of *gpr125*-injected embryos ($n=37$; Fig. 1M). Compromised anterior movement of the prechordal mesoderm relative to the overlying neural ectoderm has been proposed to cause synophthalmia or cyclopia in embryos with deficient or excess PCP pathway components (Marlow et al., 1998; Heisenberg et al., 2000; Marlow et al., 2002). At high doses of *gpr125* RNA (i.e. 400 pg), a small fraction of embryos exhibited dorsoventral axis patterning defects, including expansion of dorsal markers at 5 hpf (X.L., F.L.M. and L.S.K., unpublished) and tail truncation at 24 hpf (Fig. 1E). Therefore, Gpr125 gain-of-function phenocopies C&E defects reported for gain- and loss-of-function of PCP pathway components (Topczewski et al., 2001; Jessen et al., 2002; Marlow et al., 2002; Formstone and Mason, 2005; Carreira-Barbosa et al., 2009) and disrupts patterning only when expressed in great excess.

At the cellular level, Gpr125-Cherry overexpressing embryos had extra columns of cells in the notochord when compared with controls, indicating a deficiency in mediolateral intercalation (Fig. 1P,Q). Indeed, morphometric analysis revealed defects in mediolateral cell elongation and alignment, two PCP-dependent polarized cell behaviors essential for mediolateral intercalation (Keller et al., 2000; Gray et al., 2011). In one-somite stage control embryos, 55% of dorsal ectodermal cells oriented their long axes within a 20° arc perpendicular to the notochord and exhibited an average length-to-width ratio (LWR) of 1.72±0.04 ($n=158$; Fig. 1R), and 76% of notochord cells oriented mediolaterally with an average LWR of 2.14±0.07 ($n=131$; Fig. 1T), consistent with previous reports (Topczewski et al., 2001; Jessen et al., 2002; Marlow et al., 2002). By contrast, in *gpr125-Cherry* RNA-injected embryos, only 32% of ectodermal cells and 30% of notochord cells exhibited normal mediolateral alignment (Fig. 1S,U) and showed reduced LWRs of 1.56±0.02 ($n=266$; $P<0.001$) and 1.55±0.03 ($n=220$; $P<0.001$), respectively. In addition, we analyzed *Drosophila* Pk-GFP localization in Gpr125-overexpressing ectodermal cells (Fig. 1V-Z). Consistent with previous reports, Pk-GFP puncta preferentially localized at the anterior edge of ectodermal cells in control gastrulae (Fig. 1V,X) (Ciruna et al., 2006; Yin et al., 2008). However, in embryos overexpressing Gpr125, the percentage of cells with anterior Pk-GFP puncta decreased concomitant with an increase in cells with cytoplasmic Pk-GPF (Fig. 1W,X). These results indicate that *gpr125* gain of function impaired both molecular and morphological planar cell polarities during C&E movements.

Reduced Gpr125 enhances C&E defects of PCP mutants

To determine whether *gpr125* is essential for C&E movements, we used two antisense morpholino oligonucleotides (MOs) to disrupt its translation. Both MOs blocked translation of synthetic RNA encoding GFP fused to *gpr125* MO target sequences (supplementary material Fig. S2A-I). However, given that MO1-

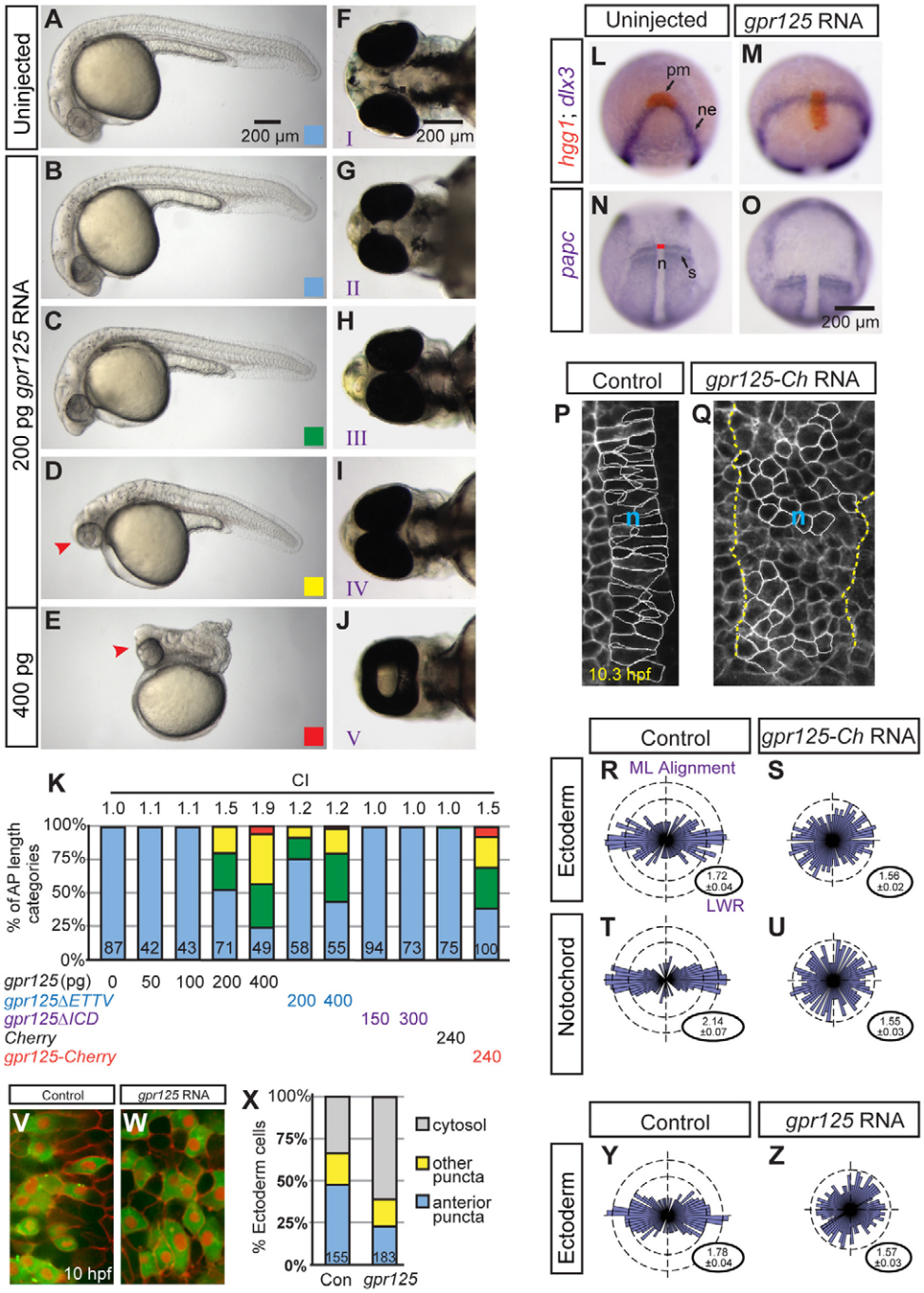

Fig. 1. Excess Gpr125 causes C&E movement defects. (**A-E**) Lateral views of uninjected or *gpr125* RNA injected embryos at 1 day post-fertilization (dpf). Anterior is leftwards. AP axis length phenotypic categories. Blue, greater than 95%; green, 80-95%; yellow, 40-79%; red, smaller than 40% of the average AP axis length of control embryos. Arrowheads in D and E indicate the cyclopic eyes and change of head position. (**F-J**) Ventral views of uninjected or *gpr125* RNA-injected embryos at 3 dpf. Anterior is leftwards. Eye fusion defects were categorized into five groups (I-V) according to Marlow et al. (Marlow et al., 1998). (**K**) Quantification of AP axis shortening and eye fusion phenotypes. The colored bars correspond to the AP axis length phenotypic categories shown in B-E. Eye fusion phenotypes were quantified by cyclopia index (CI) according to Marlow et al. (Marlow et al., 1998). CI values are above the bars and numbers of embryos analyzed inside the bars. (**L-O**) Whole-mount *in situ* hybridization analyses of marker gene expression in uninjected or 200 pg *gpr125* RNA-injected embryos at the two-somite stage. (L,M) Animal pole views, ventral upwards. (N,O) Dorsal views, anterior upwards. n, notochord; ne, neural ectoderm border; pm, prechordal mesoderm; s, somites. Red line indicates the width of the notochord at the first somites. (**P**,**Q**) mEGFP-labeled notochord (n) of control or 200 pg *gpr125-Cherry* RNA-injected embryos at the one-somite stage. Anterior is upwards. All measured notochord cells are outlined and the notochord boundary of the *gpr125*-injected embryo is marked with dashed lines. (**R-U**) Analyses of LWR and mediolateral (ML) alignment in the ectoderm or notochord of control (*n*=3 embryos, 158 and 131 cells, respectively) or 200 pg *gpr125-Cherry* RNA-injected embryos (*n*=6 embryos, 266 and 220 cells, respectively) at the one-somite stage. Rose diagrams depict cell orientation relative to the AP axis (vertical dashed line). Corresponding LWRs are expressed as mean±s.e.m. in the lower right corners. (**V**,**W**) Punctate and cytosolic distribution of Pk-GFP in control or *gpr125* RNA-injected embryos. (**X**) Classes of Pk-GFP distribution in control or *gpr125* RNA-injected embryos (155 or 183 cells, respectively). (**Y**,**Z**) ML alignment and LWR of ectodermal cells analyzed for Pk-GFP localization in control or *gpr125* RNA-injected gastrulae.

gpr125 caused non-specific cell death, which was suppressed by concurrent loss of *p53* function (supplementary material Fig. S2J,K) (Robu et al., 2007), MO2-*gpr125* was mainly used in this study. Although *gpr125* MOs did not cause specific morphological defects in wild-type embryos (supplementary material Fig. S2L-W), they enhanced the phenotypes of PCP mutants (Figs 2-4). PCP

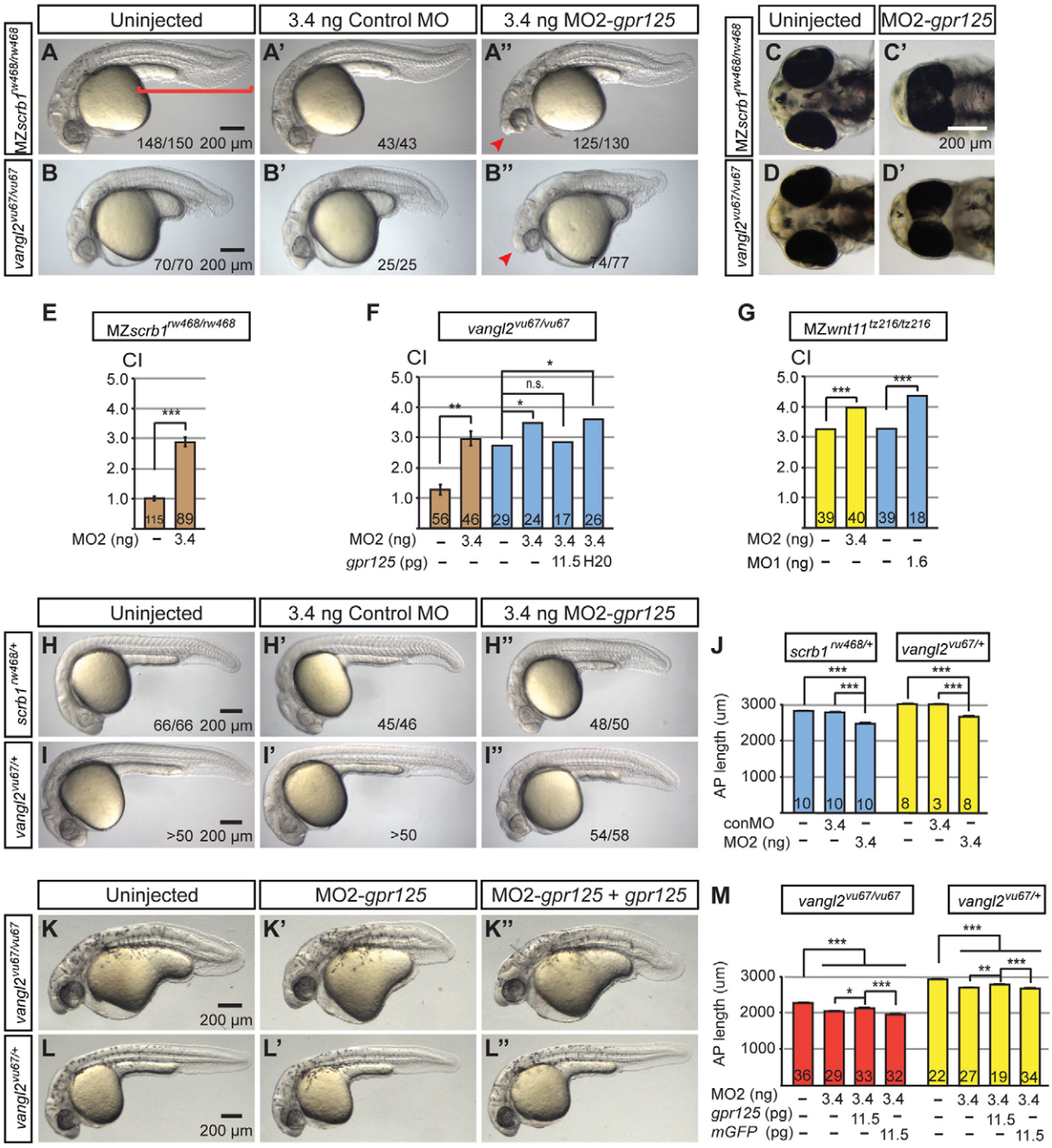

Fig. 2. Knockdown of *gpr125* enhances defects of *scrbl1/llk* and *vangl2/tri* mutants. (**A-B″**) Lateral views of uninjected, control MO- or MO2-*gpr125*-injected MZ*scrb1/llk*$^{rw468/rw468}$ or *vangl2/tri*$^{vu67/vu67}$ homozygotes at 1 dpf. Anterior is leftwards. The bracket in A marks the posterior body. Arrowheads in A″ and B″ indicate the cyclopic eyes and change of head position. Fractions of affected embryos are indicated. (**C-D′**) Ventral views of uninjected or 3.4 ng MO2-*gpr125*-injected MZ*scrb1/llk*$^{rw468/rw468}$ or *vangl2/tri*$^{vu67/vu67}$ embryos at 3 dpf. Anterior is leftwards. (**E-G**) Quantification of CI of MZ*scrb1/llk*$^{rw468/rw468}$, *vangl2/tri*$^{vu67/vu67}$ and MZ*wnt11/slb*$^{tz216/tz216}$ embryos at 3 dpf injected with *gpr125* MOs and/or RNA or water. The numbers of analyzed embryos are inside the bars. Brown bars represent results from three independent experiments with error bars indicating s.e.m. Yellow and blue bars show results from single experiments with results of additional repetitions shown in supplementary material Tables S2 and S3. *P<0.05, **P<0.01, ***P<0.001. (**H-I″**) Lateral views of uninjected, 3.4 ng control MO injected or 3.4 ng MO2-*gpr125*-injected MZ*scrb1/llk*$^{rw468/+}$ or *vangl2/tri*$^{vu67/+}$ heterozygotes at 1 dpf. Anterior is leftwards. Fractions of affected embryos are indicated, except for I and I′, where more than 50 embryos were analyzed. (**J**) Quantification of AP axis length in *scrb1/llk*$^{rw468/+}$ and *vangl2/tri*$^{vu67/+}$ embryos at 1 dpf. The numbers of analyzed embryos are inside the bars. Error bars indicate ±s.e.m. ***P<0.001. (**K-L″**) Lateral views of uninjected, 3.4 ng MO2-*gpr125*, or 3.4 ng MO2-*gpr125* and 11.5 pg *gpr125* RNA co-injected *vangl2/tri*$^{vu67/vu67}$ or *vangl2/tri*$^{vu67/+}$ embryos at 1 dpf. Anterior is leftwards. (**M**) Quantification of the impacts of *gpr125* MO and RNA on the AP axis defects of *vangl2/tri*$^{vu67/vu67}$ *vangl2/tri*$^{vu67/+}$ embryos at 1 dpf. The numbers of analyzed embryos are inside the bars. Error bars indicate ±s.e.m. *P<0.05, **P<0.01, ***P<0.001.

homozygous mutants, such as maternal-zygotic (MZ) *scribble1* (*scrb1*/*scrib*)/*landlocked* (*llk*) (Wada et al., 2005) and *vangl2/trilobtie* (*tri*) (Marlow et al., 1998; Jessen et al., 2002), exhibit shortened AP axis and variable degrees of cyclopia. Intriguingly, injection of MO2-*gpr125*, but not a control MO, further shortened the AP axis and significantly increased the penetrance and expressivity of cyclopia in these mutants (Fig. 2A-F; supplementary material Table S2). Similar enhancement of cyclopia was observed with MO1-*gpr125* and MO2-*gpr125* in MZ*wnt11/silberblick* (*slb*) homozygous mutants (Fig. 2G; supplementary material Table S3) (Heisenberg et al., 2000). Notably, MO2-*gpr125* injection caused significant shortening of the AP axis relative to uninjected or control MO-injected *scrb1/llk* and *vangl2/tri* heterozygous embryos, which do not manifest morphological C&E defects (Fig. 2H-J) (Solnica-Krezel et al., 1996; Wada et al., 2005). Supporting the specificity of MO2-*gpr125*, synthetic *gpr125* RNA lacking the MO2-*gpr125* binding site, but not water or RNA-encoding membrane EGFP (mEGFP),

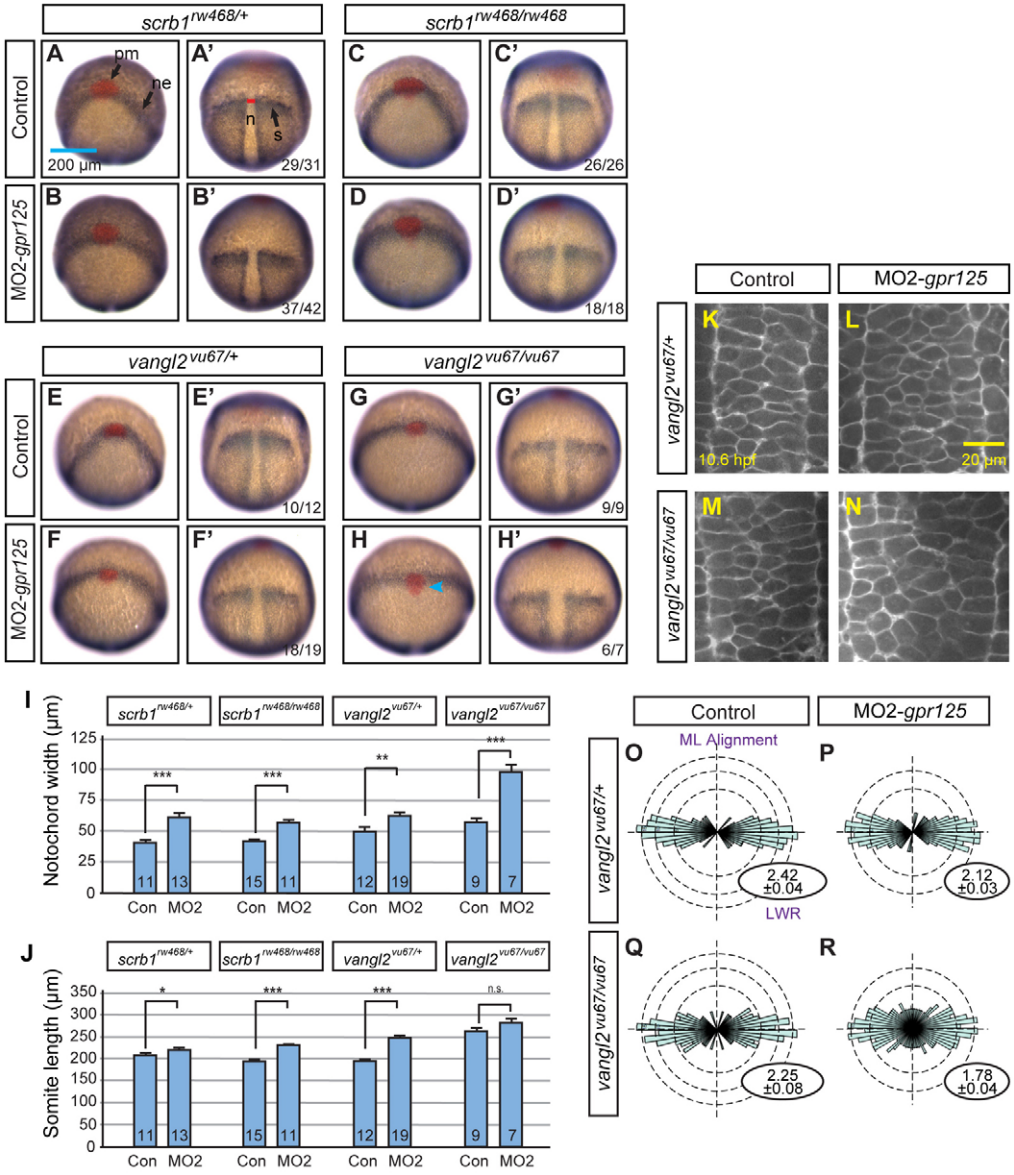

Fig. 3. Knockdown of *gpr125* enhances *scrbl1/llk* and *vangl2/tri* mutant phenotypes at the two-somite stage. (**A-H′**) Whole-mount *in situ* hybridization analyses of uninjected (A,A′) or 3.4 ng control MO-injected (C,C′,E,E′,G,G′) or 3.4 ng MO2-*gpr125*-injected (B,B′,D,D′,F,F′,H,H′) *scrb1/llk*$^{rw468/+}$, *scrb1/llk*$^{rw468/rw468}$, *vangl2/tri*$^{vu67/+}$ or *vangl2/tri*$^{vu67/vu67}$ embryos at the two-somite stage. (A-H) Animal pole views, ventral is upwards. (A′-H′) Dorsal views, anterior is upwards. n, notochord; ne, neural ectoderm border; pm, prechordal mesoderm; s, somites. Red line in A′ indicates the width of the notochord at the first somites. Arrowhead in H indicates impaired prechordal mesoderm migration. (**I**,**J**) Quantification of notochord width or first somite length at the same AP level in control (Con) or MO2-*gpr125* (MO2) injected *scrb1/llk*$^{rw468/+}$, *scrb1/llk*$^{rw468/rw468}$, *vangl2/tri*$^{vu67/+}$ or *vangl2/tri*$^{vu67/vu67}$ embryos at the two-somite stage. The numbers of analyzed embryos are inside the bars. Error bars indicate ±s.e.m. **P*<0.05, ***P*<0.01, ****P*<0.001. (**K-N**) mCherry-labeled notochord of control or MO2-*gpr125*-injected *vangl2/tri*$^{vu67/+}$ or *vangl2/tri*$^{vu67/vu67}$ embryos at the two-somite stage. (**O-R**) Analyses of LWR and ML alignment in the notochord of control or MO2-*gpr125*-injected *vangl2/tri*$^{vu67/+}$ (300 cells for control and 500 cells for MO2-*gpr125*-injected embryos) or *vangl2/tri*$^{vu67/vu67}$ (110 cells for control and 199 cells for MO2-*gpr125*-injected embryos) embryos at the two-somite stage. Rose diagrams depict cell orientation relative to the AP axis (vertical dashed line). *P*<0.0001 for *vangl2/tri*$^{vu67/+}$ samples and *P*=0.0003 for *vangl2/tri*$^{vu67/vu67}$ samples. Corresponding LWRs are expressed as mean±s.e.m. in the lower right corners. *P*<0.0001 for both groups.

significantly suppressed MO2-*gpr125* enhancement of AP axis shortening of both *vangl2/tri* homozygotes and heterozygotes (Fig. 2K-M), and cyclopia defects of *vangl2/tri* homozygotes (Fig. 2F; supplementary material Table S2). Consistent with the enhanced axis shortening at 1 dpf, MO2-*gpr125* injection caused wider and shorter neural ectoderm and axial and paraxial mesoderm in *scrb1/llk* and *vangl2/tri* homozygotes, and heterozygotes at the two-somite stage (Fig. 3A-J). At the cellular level, reduced Gpr125 function caused significant reduction of LWR and mediolateral alignment of cells in the notochord compared with control *vangl2/tri* heterozygotes and homozygotes (Fig. 3K-R). In summary, these results indicate that when PCP signaling is reduced, Gpr125 function becomes crucial for polarized cell behaviors underlying C&E.

Reduced Gpr125 enhances neuronal migration defects of *scrb1/llk* and *vangl2/tri* heterozygotes

As *scrb1/llk* and *vangl2/tri* also regulate tangential migration of FBMNs in zebrafish and mouse (Jessen et al., 2002; Carreira-Barbosa et al., 2003; Wada et al., 2005; Wada et al., 2006; Wada and Okamoto, 2009), we asked whether *gpr125* interacts with these genes in the context of FBMN migration. Although injection of MO2-*gpr125* rarely impaired FBMN migration in wild-type embryos (Fig. 4A-D), it strongly enhanced FBMN migration defects in PCP compromised genetic backgrounds (Fig. 4E-O). At 48 hpf, FBMNs migrated into rhombomere 6 (r6) and r7 in 92% of *scrb1/llk* heterozygous embryos and migrated partially into r5 and r6 in only 8% of such embryos (Fig. 4E,I). Gpr125 depletion significantly increased the number of embryos exhibiting partial FBMN migration (57%, *n*=65; Fig. 4G,I) and, strikingly, in 35% of these injected embryos, FBMNs failed to leave r4 (Fig. 4H,I). FBMN migration defects were similarly enhanced in *vangl2/tri* heterozygous embryos (Fig. 4J-O). By contrast, injection of control MOs at equivalent doses had no effect on FBMN migration in either genetic background (Fig. 4F,I,L,M,O). Therefore, *gpr125* interacts with PCP genes to promote FBMN migration.

Gpr125 recruits Dvl-GFP to membrane subdomains via direct interaction

Functional interactions between Gpr125 and PCP components and planar polarity defects of Gpr125 overexpressing gastrulae are consistent with a role of Gpr125 in modulating Wnt/PCP signaling. As Dvl membrane translocation is a prerequisite for vertebrate Wnt/PCP signaling (Park et al., 2005) and Gpr125 contains a PDZ binding motif (supplementary material Fig. S1), we tested whether Gpr125 influenced Dvl subcellular localization using previously described membrane recruitment assays (Carreira-Barbosa et al., 2003; Witzel et al., 2006). Synthetic RNA encoding *Xenopus* Dvl-GFP and zebrafish Gpr125 were injected at the one-cell stage and Dvl-GFP distribution was assayed at the late blastula stage (4-5 hpf), prior to PCP signaling-dependent mediolateral cell polarization (Topczewski et al., 2001; Jessen et al., 2002; Marlow et al., 2002; Tada and Kai, 2009; Yin et al., 2009). Consistent with previous reports (Wallingford et al., 2000; Carreira-Barbosa et al., 2003; Witzel et al., 2006), Dvl-GFP mainly formed cytoplasmic puncta when expressed alone (*n*=20/20; Fig. 5A-A″). By contrast, when co-expressed with Gpr125, Dvl-GFP occupied patch-like subdomains at cell membranes (*n*=36/36; Fig. 5B-B″). Gpr125 mutant protein lacking the C-terminal ETTV peptide (*gpr125ΔETTV*) resulted in less prominent Dvl-GFP patches (*n*=13/13; Fig. 5C-C″). As quantified in Fig. 5E,F, ΔETTV recruited less Dvl-GFP to the membrane compared with the full-length receptor, and the Dvl-GFP subdomain size shifted towards smaller categories. Consistent with its reduced activity in Dvl membrane recruitment assays, Gpr125ΔETTV overexpression induced C&E defects with lower penetrance and severity than full-length Gpr125 (Fig. 1K). When the entire intracellular domain of Gpr125 was deleted (Gpr125ΔICD), no Dvl-GFP recruitment was observed in co-expression experiments (*n*=18/18; Fig. 5D-D″). Consistently, Gpr125ΔICD did not disrupt C&E at doses equivalent to the effective doses of RNA encoding full-length Gpr125 (Fig. 1K).

To test for direct binding between Dvl and Gpr125 intracellular domain (Gpr125ICD), we performed pull-down experiments with

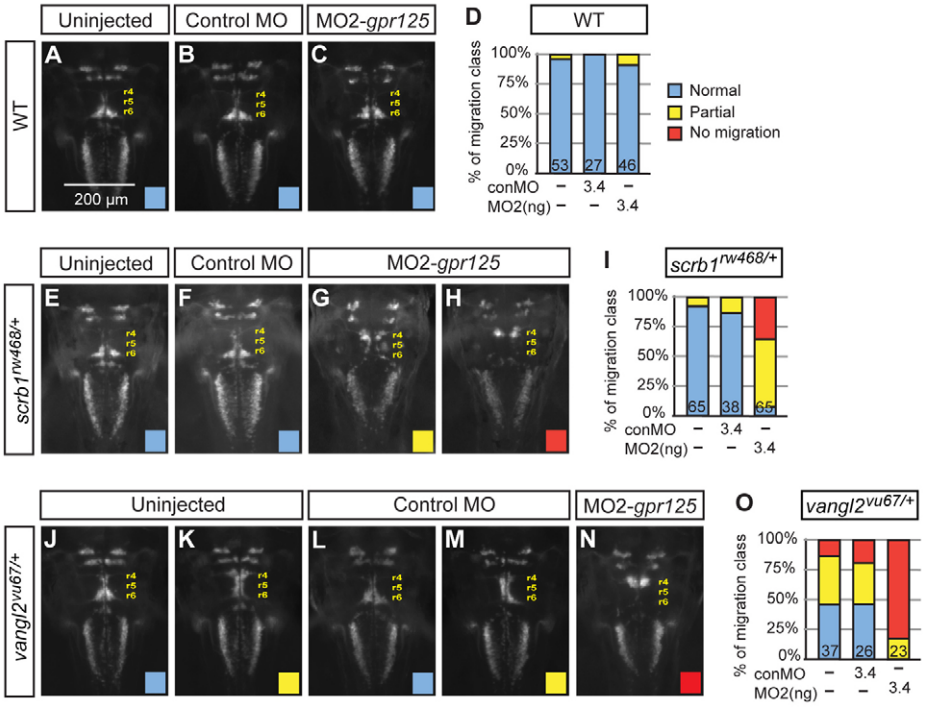

Fig. 4. *gpr125* interacts with *scrb1/llk* and *vangl2/tri* in FBMN migration. (**A-C**) Dorsal views of *islet1*(*isl1*):*GFP*-expressing neurons in uninjected, 3.4 ng control MO or 3.4 ng MO2-*gpr125* injected wild-type siblings of *scrb1/llk* or *vangl2/tri* heterozygous embryos at 48 hpf. Anterior is upwards. r4 (rhombomere 4), r5 and r6 positions are labeled. (**D**) Frequency of FBMN migration phenotypic classes observed in wild-type embryos. Blue, normal; yellow, partial; red, no migration. (**E-H**) Dorsal views of *isl1:GFP*-expressing neurons in uninjected, 3.4 ng control MO or 3.4 ng MO2-*gpr125*-injected *scrb1/llk*$^{rw468/+}$ embryos at 48 hpf. (**I**) Frequency of the FBMN migration phenotypic classes observed in *scrb1/llk*$^{rw468/+}$ embryos. (**J-N**) Dorsal views of *isl1:GFP*-expressing neurons in uninjected, 3.4 ng control MO or 3.4 ng MO2-*gpr125*-injected *vangl2/tri*$^{vu67/+}$ embryos at 48 hpf. (**O**) Frequency of FBMN migration phenotypic classes observed in *vangl2/tri*$^{vu67/+}$ heterozygotes.

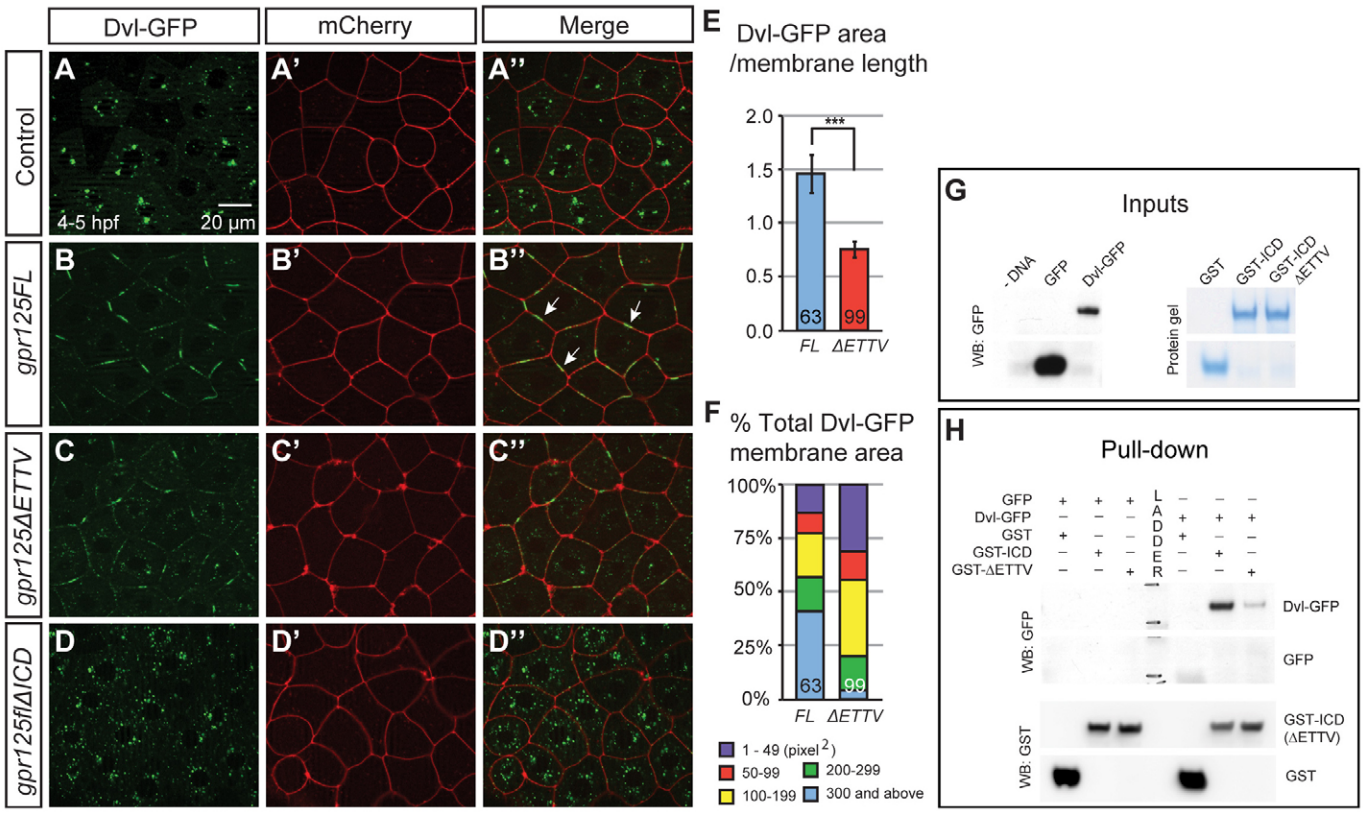

Fig. 5. Gpr125 promotes Dvl-GFP localization in discrete membrane subdomains via direct interaction. (**A-D″**) Animal pole views of live embryos at 4-5 hpf co-injected with 150 pg *dvl-GFP* and 50 pg *mCherry* RNA in the absence (A-A″) and presence of 380 pg *gpr125FL* (B-B″), *gpr125ΔETTV* (C-C″) or *gpr125ΔICD* RNA (D-D″). Arrows in B″ indicate Dvl-GFP membrane subdomains. (**E**) Ratio of Dvl-GFP membrane area to the length of the membrane measured on embryos expressing full-length or ΔETTV Gpr125. Numbers of membranes analyzed are inside bars. Data are mean±s.e.m. ***P<0.001. (**F**) Size distribution of Dvl-GFP membrane subdomains in embryos expressing full-length or ΔETTV Gpr125. Numbers of membranes analyzed are inside bars. (**G**,**H**) Pull-down assay with GST- and GFP-fusion proteins. Ten percent of GFP-fusion protein inputs were blotted with anti-GFP antibody and 100% GST fusion protein inputs were stained with Denville Blue Protein Stain (G). Pull-down results were analyzed by western blotting using anti-GFP and anti-GST antibodies (H).

purified GST-Gpr125ICD, GST-Gpr125ICDΔETTV fusion proteins and *in vitro* translated *Xenopus* Dvl-GFP (Fig. 5G,H). We found that GST-Gpr125ICD pulled down Dvl-GFP, indicative of a direct interaction. The ΔETTV form pulled down less Dvl-GFP (Fig. 5H), suggesting that ETTV promotes Gpr125ICD binding to Dvl. Taken together, our results suggest that Gpr125 modulates PCP signaling by interacting with Dvl and promoting its accumulation in membrane subdomains.

Dvl clusters Gpr125 and select PCP components into membrane subdomains

Cytoplasmic core PCP components, including Dvl, cluster PCP complexes in the cell membranes of *Drosophila* pupal wings (Strutt et al., 2011). Given that Dvl-GFP localized to membrane subdomains when co-expressed with Gpr125, we asked whether Gpr125 colocalized with Dvl in these membrane subdomains using a Gpr125 C-terminal Cherry fusion protein (Gpr125-Cherry), which, when overexpressed, impaired C&E movements and underlying cell polarity similarly to the wild-type protein (Fig. 1K,Q,S,U). In zebrafish blastulae, Gpr125-Cherry expressed alone displayed uniform membrane distribution (n=17/17; Fig. 6A-A″), but it colocalized with Dvl-GFP in prominent membrane subdomains in co-expression experiments (n=12/12; Fig. 6B-B″; supplementary material Movie 1). Similarly, when co-expressed, Dvl-GFP clustered Gpc4/Kny-GFP into membrane subdomains in late blastulae (n=10/12, Fig. 6D-D″; supplementary material Movie 2). Interestingly, these Dvl-mediated PCP membrane subdomains preferentially localized at the central regions of cell contacts between neighboring blastomeres (Fig. 6E). In addition, Dvl-GFP promoted uniform membrane localization of endogenous Vangl2/Tri in late blastulae (n=4/5; Fig. 6G″), when endogenous Tri/Vangl2 was mainly cytoplasmic in uninjected embryos (Fig. 6F).

Next, we investigated whether Gpr125 influenced the distribution of other PCP components, including Fzd7-CFP, Gpc4/Kny-GFP and endogenous Vangl2 in blastulae expressing Gpr125-Cherry, but no change of their distribution was observed (supplementary material Fig. S3). By contrast, when co-expressed with Dvl-YFP, Gpr125-Cherry, Fzd7-CFP and Dvl-YFP colocalized in membrane subdomains (n=17/22; Fig. 7A-A″). Moreover, mosaic expression of Gpr125 enhanced Gpc4/Kny-GFP clustering when Dvl was overexpressed (n=6/10; Fig. 7B-B″). In contrast to Fzd7 and Gpc4, neither endogenous nor overexpressed zebrafish Vangl2 was enriched in Gpr125-Cherry and Dvl-GFP-containing subdomains (C-F; n=15/15 for endogenous Vangl2; n=5/5 for overexpressed Vangl2). These results suggest that, analogous to *Drosophila*, distinct PCP complexes can form in vertebrates, and Fzd7 and Gpc4/Kny may be components of large Dvl-containing protein complexes, the formation of which is promoted by Gpr125.

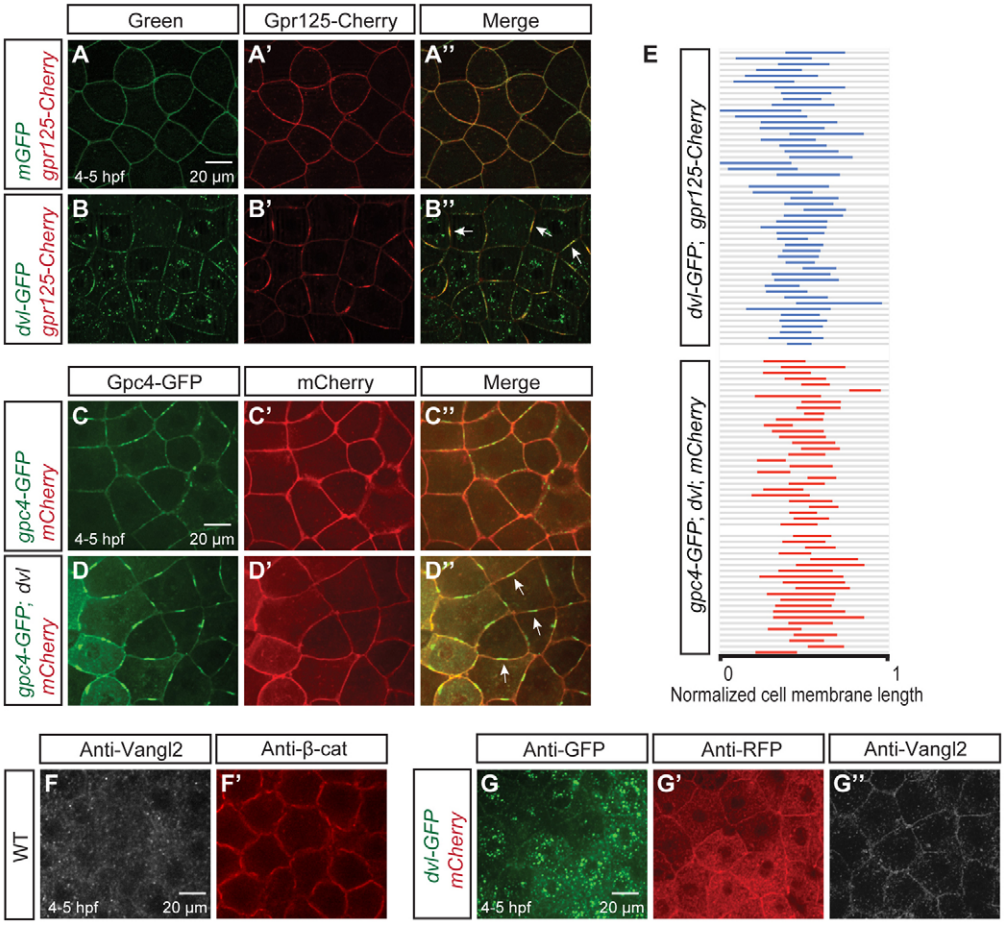

Fig. 6. Dvl clusters Gpr125 and Gpc4/Kny into membrane subdomains and promotes uniform Vangl2/Tri membrane localization in late blastulae (4-5 hpf). (**A-B″**) Animal pole views of live blastulae co-injected with 267 pg *gpr125-Cherry* RNA and either 150 pg *mEGFP* RNA (A-A″) or 150 pg *dvl-GFP* RNA (B-B″). Arrows in B″ indicate Gpr125-Cherry:Dvl-GFP membrane subdomains. (**C-D″**) Animal pole views of live blastulae co-injected with 60 pg *gpc4/kny-GFP* RNA, 50 pg *mCherry* RNA (C-C″) and 150 pg *dvl* RNA (D-D″). Arrows in D″ indicate Gpc4/Kny-GFP membrane subdomains. (**E**) Graphic representation of the relative distribution of Dvl-GFP:Gpr125-Cherry and Gpc4/Kny-GFP:Dvl subdomains along cell membranes. Membrane length was normalized as one. (**F**,**F′**) Animal pole views of a whole-mount immunostained wild-type blastula with Vangl2 and β-catenin antibodies. (**G-G″**) Animal pole views of a 50 pg *mCherry* and 150 pg *dvl-GFP* RNA-injected blastula immunostained for GFP, RFP and Vangl2.

To assess the interaction between Gpr125, Dvl and Vangl2 during C&E movements, we examined the relative distribution of Gpr125-Cherry, Dvl-GFP and endogenous Vangl2 at 10 hpf. Gpr125-Cherry localized to cell membranes and formed puncta both on the membrane and in the cytosol (Fig. 8A′,A″). Endogenous Vangl2 localized mainly to the cell membranes (Fig. 8B) and membrane staining was not observed in MZ*vang/tri*$^{vu67/vu67}$ mutants (Fig. 8C). Intriguingly, when co-expressed during gastrulation, Gpr125-Cherry and Dvl-GFP colocalized in large membrane patches, but endogenous Vangl2 was not enriched in Gpr125-Cherry:Dvl-GFP patches (Fig. 8D-F″). Therefore, Gpr125 might primarily interact with Dvl-containing protein complexes during C&E movements.

DISCUSSION

Previously, the expression of *Gpr125* was reported in various tissues of mouse embryos and adults, including the pluripotent spermatogonial progenitor cells (Seandel et al., 2007; Homma et al., 2009; Pickering et al., 2008); however, its function was not known. Here, we have identified zebrafish Gpr125 as a novel modulator of C&E gastrulation movements and tangential FBMN migration, two processes evolutionarily conserved among vertebrates that require PCP signaling (Wada and Okamoto, 2009; Gray et al., 2011). Towards elucidating the genetic and cellular mechanisms by which Gpr125 regulates these processes, we showed that excess Gpr125 impaired Wnt/PCP-dependent cellular polarities underlying normal C&E gastrulation movements. Moreover, reduction of *gpr125* expression exacerbated C&E and neuronal migration defects of several Wnt/PCP component mutants. At the molecular level, we showed that Gpr125 interacted with and recruited Dvl into membrane subdomains, and promoted accumulation of select PCP components in such membrane subdomains.

We created a *gpr125* loss-of-function condition with two antisense MOs, which effectively blocked translation of synthetic RNA encoding GFP fused to *gpr125* MO target sequences. However, the effectiveness of the MOs in blocking translation of endogenous Gpr125 protein could not be evaluated because Gpr125 antibodies are unavailable. Nevertheless, these MOs probably created at least a partial loss-of-function condition, as they enhanced the C&E gastrulation and FBMN migration defects of homozygous and heterozygous PCP mutants, whereas a control MO did not (Figs 2-4). Similar to the interaction between *gpr125* and PCP pathway genes reported here, exacerbation of C&E defects has been reported for compound PCP pathway mutants compared with single mutants (Marlow et al., 1998; Carreira-Barbosa et al., 2003; Kilian et al., 2003). More importantly, co-injecting *gpr125* RNA lacking the MO targeting sequence partially suppressed the exacerbated C&E defects in MO2-*gpr125*-injected PCP mutants. Similar to *gpr125* MO-injected wild-type zebrafish embryos, *Gpr125* knock-in null mice are grossly normal and fertile (Seandel et al., 2007). As *gpr125* RNA is maternally deposited and we could not determine the abundance of maternal protein, the lack of early developmental defects in *gpr125* morphants could be due to maternal protein contribution. Alternatively, as observed for *celsr/flamingo* genes, redundancy with other adhesion GPCRs or PCP pathway components might mask the loss of Gpr125 function (Carreira-Barbosa et al., 2009).

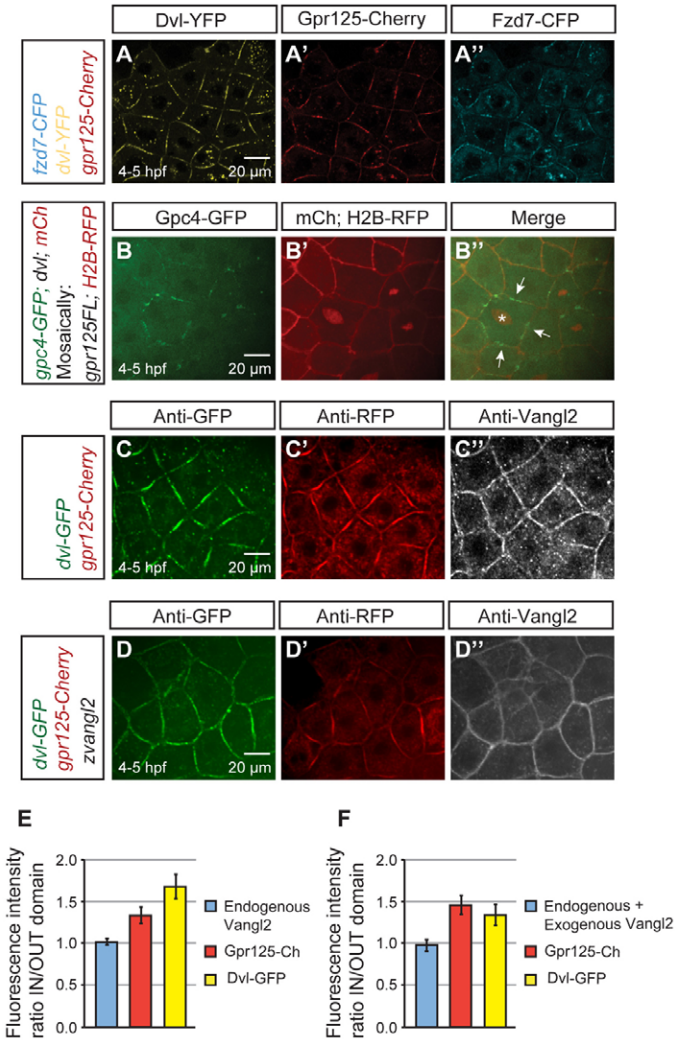

Fig. 7. Gpr125 promotes localization of select PCP components in Dvl-containing membrane subdomains in late blastulae (4-5 hpf). (**A-A″**) Live blastula co-injected with 110 pg *fzd7-CFP*, 150 pg *dvl-YFP* and 300 pg *gpr125-Cherry* RNA. (**B-B″**) Live blastula co-injected with 60 pg *gpc4/kny-GFP*, 150 pg *dvl* and 50 pg *mCherry* at the one-cell stage, and 4 pg *H2B-RFP* and 20 pg *gpr125FL* RNA in one blastomere at the 16- to ~32-cell stage. The star in B″ marks an H2B-RFP-positive nucleus and arrows indicate membrane subdomains. (**C-D″**) Blastula injected with 300 pg *gpr125-Cherry*, 150 pg *dvl-GFP* (C-C″) and 50 pg zebrafish *vangl2/tri* RNA (D-D″) immunostained for GFP, RFP and Vangl2. Animal pole views in A-D. (**E**,**F**) Quantification of fluorescence intensity ratios inside/outside domain for Vangl2, Gpr125-Cherry and Dvl-GFP in embryos injected with 300 pg *gpr125-Cherry*, 150 pg *dvl-GFP* (E) and 50 pg zebrafish *vangl2* RNA (F). Data are mean±s.e.m.

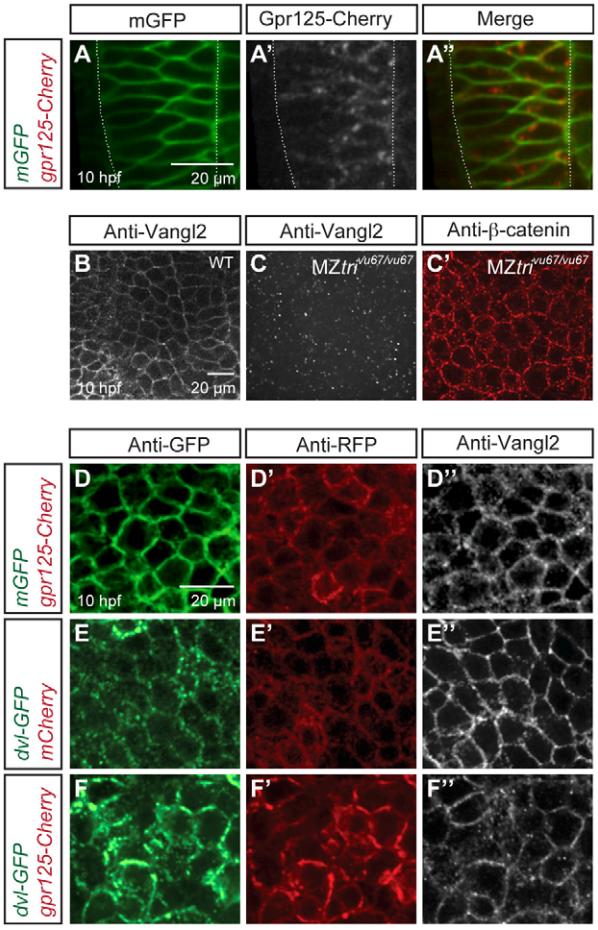

Fig. 8. Gpr125-Cherry and Dvl-GFP colocalize during gastrulation (10 hpf). (**A-A″**) Dorsal views of a gastrula injected with 50 pg *gpr125-Cherry* and 150 pg *mEGFP* RNA. Broken white lines outline the notochord. (**B-C′**) Whole-mount immunostaining for endogenous Vangl2 and β-catenin in wild-type (B) or MZ*vang/tri*$^{vu67/vu67}$ gastrulae (C-C′). (**D-F″**) Dorsal mesoderm of gastrulae co-injected with 150 pg *mEGFP* and 300 pg *gpr125-Cherry* RNA (D-D″), 150 pg *dvl-GFP* and 50 pg *mCherry* RNA (E-E″), or 150 pg *dvl-GFP* RNA and 300 pg *gpr125-Cherry* RNA (F-F″), and immunostained for GFP, RFP and Vangl2.

We showed that the Gpr125 intracellular domain interacted directly with Dvl in pull-down experiments (Fig. 5) and was required for Dvl recruitment into membrane subdomains upon Gpr125 overexpression in zebrafish blastula (Fig. 5). Given that Dvl membrane translocation is essential for vertebrate Wnt/PCP signaling (Park et al., 2005) and C&E movements are altered by excess PCP components (Wallingford et al., 2000; Topczewski et al., 2001; Jessen et al., 2002; Marlow et al., 2002; Carreira-Barbosa et al., 2003; Formstone and Mason, 2005), this interaction probably in part accounts for C&E defects caused by Gpr125 gain of function and possibly the exacerbated C&E defects caused by Gpr125 loss of function in PCP mutants. Interestingly, we did not detect significant differences in mediolateral elongation or cell orientation among cells with distinct Pk distribution patterns in either control gastrulae or those overexpressing Gpr125 (data not shown). Moreover, we observed little change in Pk-GFP distribution due to Gpr125 depletion in both wild type and *vangl2/tri* heterozygotes (data not shown). Therefore, it is plausible that Pk does not interact directly with Gpr125. It will be important to examine whether Gpr125 loss of function would influence Dvl distribution. As Dvl is not required for FBMN migration (Jessen et al., 2002; Wada and Okamoto, 2009), Gpr125 and the relevant PCP components probably regulate FBMN migration and C&E via distinct mechanisms.

We found that the PDZ-binding motif of Gpr125 was partially responsible for Dvl binding and recruitment (Fig. 5). The requirement of the PDZ-binding motif for Dvl binding varies among different proteins. It is dispensable for binding of Fzd or Vangl2/Tri to Dvl (Umbhauer et al., 2000; Park and Moon, 2002; Wong et al., 2003). However, the PDZ-binding motif mediates direct binding

between *Xenopus* Dvl and its cytoplasmic interacting protein Dapper/Dact (Cheyette et al., 2002; Gloy et al., 2002; Wong et al., 2003; Teran et al., 2009). As in Gpr125, the Dapper PDZ-binding motif, is –TTV and the threonine at the −2 position is reported to be within hydrogen bonding distance of a highly conserved arginine 325 residue present in Dvl proteins, and is also essential for Dvl interaction with Dapper (Cheyette et al., 2002). Additional Gpr125 motif(s) mediating Dvl binding remain to be defined.

Previous reports show that Fzd7 recruits Dvl uniformly to the cell membrane when overexpressed in the zebrafish blastula and promotes Dvl accumulation into discrete membrane subdomains when co-expressed with Wnt11 (Witzel et al., 2006). We observed that Dvl clustered Gpr125 into membrane subdomains, and vice versa, even without co-expression of Wnt11 (Figs 5, 6). Notably, Gpr125 promoted accumulation of Fzd7 and Gpc4/Kny in the subdomains (Fig. 7). These observations are consistent with a recently discovered role for endogenous Dsh in clustering PCP complexes into membrane subdomains in *Drosophila* wing epithelia (Strutt et al., 2011). Moreover, our study raises the possibility that other proteins such as Gpr125 cooperate with Dvl to promote formation of such membrane subdomains. Interestingly, *Drosophila* Pk forms membrane clusters when co-expressed with *Xenopus* Vangl2 in *Xenopus* animal cap explants (Jenny et al., 2003), but in zebrafish blastula, Pk co-expression inhibits Fzd7-mediated recruitment of Dvl to the cell membrane possibly by destabilizing Dvl (Carreira-Barbosa et al., 2003). Based on additional evidence that Pk and Dvl fusion proteins localize to opposing cell edges in zebrafish gastrula (Ciruna et al., 2006; Yin et al., 2008), it is tempting to speculate that distinct clusters of endogenous PCP complexes might exist during C&E movements in vertebrates. Moreover, because the membrane subdomains containing Gpr125 and Dvl were enriched in Fzd and Gpc4/Kny but not in Vangl2/Tri, it is also possible that Gpr125 could be involved in formation of asymmetric PCP complexes. As proposed for *Drosophila* PCP signaling, clustering of PCP complexes could afford a self-enhancement mechanism contributing to the establishment and/or maintenance of planar polarity (Strutt et al., 2011). During C&E in particular, as mesenchymal cells are moving and changing their contacts rather frequently, the local organization of PCP proteins into subdomains could facilitate efficient establishment of planar polarity in the context of dynamic cell rearrangements.

It is unclear how clustering of PCP complexes might contribute to polarized cell behaviors driving C&E movements. Nevertheless, formation of Wnt11:Fzd7:Dvl subdomains has been correlated with increased persistence of membrane contacts. In addition, Celsrs have been demonstrated to contribute substantially to this effect, likely via their ability to mediate adhesion (Usui et al., 1999; Shima et al., 2004; Witzel et al., 2006). Like Celsrs, Gpr125 is an adhesion GPCR and its extracellular domain contains protein modules known to mediate protein-ligand interactions suitable for regulating intercellular communication and cell adhesion (de Wit et al., 2011; Pal et al., 2012). Therefore, it is worth testing in the future whether Gpr125 might function in PCP subdomains to regulate cell adhesion.

In summary, we identified zebrafish Gpr125 as a novel modulator of C&E gastrulation movements and tangential FBMN migration. Gpr125 influences Wnt/PCP pathway activity in part via interacting with and modulating the distribution of Dvl. Our discovery that Gpr125 contributes to C&E during gastrulation, a processes where all known PCP components act, and later during FBMN migration, where only a subset of PCP genes are required, opens up exciting avenues for further studies of Gpr125 function, in particular towards understanding how Wnt/PCP signaling regulates cell and tissue polarity in distinct contexts.

Acknowledgements
We thank Drs Andreas Jenny, Carl-Philipp Heisenberg, Fang Lin, Hitoshi Okamoto, John Wallingford, Lei Feng and Avik Choudhuri for their generosity in sharing reagents and fish lines; Drs Andreas Jenny, Adrian Santos-Ledo, Kelly Monk and Ryan S. Gray for comments on the manuscript; Linda Lobos for editing; and Analytical Imaging Facility at Albert Einstein College of Medicine, Dr Y. G. Yeung, and F.L.M. and L.S.K. lab members for helpful discussions and technical support. We acknowledge the research assistants in our fish facilities for fish care.

Funding
This work was supported in part by National Institutes of Health grants [R01GM089979 to F.L.M. and R01GM77770 and GM55101 to L.S.K.]. Deposited in PMC for release after 12 months.

Competing interests statement
The authors declare no competing financial interests.

Author contributions
All authors conceived and designed the experiments, analyzed and discussed the data, and discussed the manuscript. X.L., I.R., D.S.S. and M.N. performed the experiments. H.E.H., F.L.M. and L.S.-K. contributed reagents, materials and analysis tools. X.L. wrote the manuscript with the assistance of L.S.-K., F.L.M., I.R. and D.S.S.

Supplementary material
Supplementary material available online at
http://dev.biologists.org/lookup/suppl/doi:10.1242/dev.094839/-/DC1

References

Axelrod, J. D. (2001). Unipolar membrane association of Dishevelled mediates Frizzled planar cell polarity signaling. *Genes Dev.* **15**, 1182-1187.
Bastock, R., Strutt, H. and Strutt, D. (2003). Strabismus is asymmetrically localised and binds to Prickle and Dishevelled during Drosophila planar polarity patterning. *Development* **130**, 3007-3014.
Berghmans, S., Murphey, R. D., Wienholds, E., Neuberg, D., Kutok, J. L., Fletcher, C. D., Morris, J. P., Liu, T. X., Schulte-Merker, S., Kanki, J. P. et al. (2005). tp53 mutant zebrafish develop malignant peripheral nerve sheath tumors. *Proc. Natl. Acad. Sci. USA* **102**, 407-412.
Carreira-Barbosa, F., Concha, M. L., Takeuchi, M., Ueno, N., Wilson, S. W. and Tada, M. (2003). Prickle 1 regulates cell movements during gastrulation and neuronal migration in zebrafish. *Development* **130**, 4037-4046.
Carreira-Barbosa, F., Kajita, M., Morel, V., Wada, H., Okamoto, H., Martinez Arias, A., Fujita, Y., Wilson, S. W. and Tada, M. (2009). Flamingo regulates epiboly and convergence/extension movements through cell cohesive and signalling functions during zebrafish gastrulation. *Development* **136**, 383-392.
Cheyette, B. N., Waxman, J. S., Miller, J. R., Takemaru, K., Sheldahl, L. C., Khlebtsova, N., Fox, E. P., Earnest, T. and Moon, R. T. (2002). Dapper, a Dishevelled-associated antagonist of beta-catenin and JNK signaling, is required for notochord formation. *Dev. Cell* **2**, 449-461.
Ciruna, B., Jenny, A., Lee, D., Mlodzik, M. and Schier, A. F. (2006). Planar cell polarity signalling couples cell division and morphogenesis during neurulation. *Nature* **439**, 220-224.
de Wit, J., Hong, W., Luo, L. and Ghosh, A. (2011). Role of leucine-rich repeat proteins in the development and function of neural circuits. *Annu. Rev. Cell Dev. Biol.* **27**, 697-729.
Feiguin, F., Hannus, M., Mlodzik, M. and Eaton, S. (2001). The ankyrin repeat protein Diego mediates Frizzled-dependent planar polarization. *Dev. Cell* **1**, 93-101.
Formstone, C. J. and Mason, I. (2005). Combinatorial activity of Flamingo proteins directs convergence and extension within the early zebrafish embryo via the planar cell polarity pathway. *Dev. Biol.* **282**, 320-335.
Fredriksson, R., Lagerström, M. C., Lundin, L. G. and Schiöth, H. B. (2003). The G-protein-coupled receptors in the human genome form five main families. Phylogenetic analysis, paralogon groups, and fingerprints. *Mol. Pharmacol.* **63**, 1256-1272.
Gloy, J., Hikasa, H. and Sokol, S. Y. (2002). Frodo interacts with Dishevelled to transduce Wnt signals. *Nat. Cell Biol.* **4**, 351-357.
Goodrich, L. V. and Strutt, D. (2011). Principles of planar polarity in animal development. *Development* **138**, 1877-1892.
Gray, R. S., Roszko, I. and Solnica-Krezel, L. (2011). Planar cell polarity: coordinating morphogenetic cell behaviors with embryonic polarity. *Dev. Cell* **21**, 120-133.

Heisenberg, C. P., Tada, M., Rauch, G. J., Saúde, L., Concha, M. L., Geisler, R., Stemple, D. L., Smith, J. C. and Wilson, S. W. (2000). Silberblick/Wnt11 mediates convergent extension movements during zebrafish gastrulation. *Nature* **405**, 76-81.
Hering, H. and Sheng, M. (2002). Direct interaction of Frizzled-1, -2, -4, and -7 with PDZ domains of PSD-95. *FEBS Lett.* **521**, 185-189.
Homma, S., Shimada, T., Hikake, T. and Yaginuma, H. (2009). Expression pattern of LRR and Ig domain-containing protein (LRRIG protein) in the early mouse embryo. *Gene Expr. Patterns* **9**, 1-26.
Jenny, A., Darken, R. S., Wilson, P. A. and Mlodzik, M. (2003). Prickle and Strabismus form a functional complex to generate a correct axis during planar cell polarity signaling. *EMBO J.* **22**, 4409-4420.
Jessen, J. R., Topczewski, J., Bingham, S., Sepich, D. S., Marlow, F., Chandrasekhar, A. and Solnica-Krezel, L. (2002). Zebrafish trilobite identifies new roles for Strabismus in gastrulation and neuronal movements. *Nat. Cell Biol.* **4**, 610-615.
Keller, R., Davidson, L., Edlund, A., Elul, T., Ezin, M., Shook, D. and Skoglund, P. (2000). Mechanisms of convergence and extension by cell intercalation. *Philos. Trans. R. Soc. B* **355**, 897-922.
Kilian, B., Mansukoski, H., Barbosa, F. C., Ulrich, F., Tada, M. and Heisenberg, C. P. (2003). The role of Ppt/Wnt5 in regulating cell shape and movement during zebrafish gastrulation. *Mech. Dev.* **120**, 467-476.
Kimmel, C. B., Ballard, W. W., Kimmel, S. R., Ullmann, B. and Schilling, T. F. (1995). Stages of embryonic development of the zebrafish. *Dev. Dyn.* **203**, 253-310.
Kuhnert, F., Mancuso, M. R., Shamloo, A., Wang, H. T., Choksi, V., Florek, M., Su, H., Fruttiger, M., Young, W. L., Heilshorn, S. C. et al. (2010). Essential regulation of CNS angiogenesis by the orphan G protein-coupled receptor GPR124. *Science* **330**, 985-989.
Lin, F., Sepich, D. S., Chen, S., Topczewski, J., Yin, C., Solnica-Krezel, L. and Hamm, H. (2005). Essential roles of Galpha12/13 signaling in distinct cell behaviors driving zebrafish convergence and extension gastrulation movements. *J. Cell Biol.* **169**, 777-787.
Lin, F., Chen, S., Sepich, D. S., Panizzi, J. R., Clendenon, S. G., Marrs, J. A., Hamm, H. E. and Solnica-Krezel, L. (2009). Galpha12/13 regulate epiboly by inhibiting E-cadherin activity and modulating the actin cytoskeleton. *J. Cell Biol.* **184**, 909-921.
Marlow, F., Zwartkruis, F., Malicki, J., Neuhauss, S. C., Abbas, L., Weaver, M., Driever, W. and Solnica-Krezel, L. (1998). Functional interactions of genes mediating convergent extension, knypek and trilobite, during the partitioning of the eye primordium in zebrafish. *Dev. Biol.* **203**, 382-399.
Marlow, F., Topczewski, J., Sepich, D. and Solnica-Krezel, L. (2002). Zebrafish Rho kinase 2 acts downstream of Wnt11 to mediate cell polarity and effective convergence and extension movements. *Curr. Biol.* **12**, 876-884.
McNeill, H. (2010). Planar cell polarity: keeping hairs straight is not so simple. *Cold Spring Harb. Perspect. Biol.* **2**, a003376.
Monk, K. R., Naylor, S. G., Glenn, T. D., Mercurio, S., Perlin, J. R., Dominguez, C., Moens, C. B. and Talbot, W. S. (2009). A G protein-coupled receptor is essential for Schwann cells to initiate myelination. *Science* **325**, 1402-1405.
Monk, K. R., Oshima, K., Jörs, S., Heller, S. and Talbot, W. S. (2011). Gpr126 is essential for peripheral nerve development and myelination in mammals. *Development* **138**, 2673-2680.
Myers, D. C., Sepich, D. S. and Solnica-Krezel, L. (2002). Bmp activity gradient regulates convergent extension during zebrafish gastrulation. *Dev. Biol.* **243**, 81-98.
Pal, K., Melcher, K. and Xu, H. E. (2012). Structure and mechanism for recognition of peptide hormones by Class B G-protein-coupled receptors. *Acta Pharmacol. Sin.* **33**, 300-311.
Park, M. and Moon, R. T. (2002). The planar cell-polarity gene stbm regulates cell behaviour and cell fate in vertebrate embryos. *Nat. Cell Biol.* **4**, 20-25.
Park, T. J., Gray, R. S., Sato, A., Habas, R. and Wallingford, J. B. (2005). Subcellular localization and signaling properties of dishevelled in developing vertebrate embryos. *Curr. Biol.* **15**, 1039-1044.
Piao, X., Hill, R. S., Bodell, A., Chang, B. S., Basel-Vanagaite, L., Straussberg, R., Dobyns, W. B., Qasrawi, B., Winter, R. M., Innes, A. M. et al. (2004). G protein-coupled receptor-dependent development of human frontal cortex. *Science* **303**, 2033-2036.
Pickering, C., Hägglund, M., Szmydynger-Chodobska, J., Marques, F., Palha, J. A., Waller, L., Chodobski, A., Fredriksson, R., Lagerström, M. C. and Schiöth, H. B. (2008). The Adhesion GPCR GPR125 is specifically expressed in the choroid plexus and is upregulated following brain injury. *BMC Neurosci.* **9**, 97.
Robu, M. E., Larson, J. D., Nasevicius, A., Beiraghi, S., Brenner, C., Farber, S. A. and Ekker, S. C. (2007). p53 activation by knockdown technologies. *PLoS Genet.* **3**, e78.
Schindelin, J., Arganda-Carreras, I., Frise, E., Kaynig, V., Longair, M., Pietzsch, T., Preibisch, S., Rueden, C., Saalfeld, S., Schmid, B. et al. (2012). Fiji: an open-source platform for biological-image analysis. *Nat. Methods* **9**, 676-682.
Seandel, M., James, D., Shmelkov, S. V., Falciatori, I., Kim, J., Chavala, S., Scherr, D. S., Zhang, F., Torres, R., Gale, N. W. et al. (2007). Generation of functional multipotent adult stem cells from GPR125+ germline progenitors. *Nature* **449**, 346-350.
Shima, Y., Kengaku, M., Hirano, T., Takeichi, M. and Uemura, T. (2004). Regulation of dendritic maintenance and growth by a mammalian 7-pass transmembrane cadherin. *Dev. Cell* **7**, 205-216.
Simons, M. and Mlodzik, M. (2008). Planar cell polarity signaling: from fly development to human disease. *Annu. Rev. Genet.* **42**, 517-540.
Solnica-Krezel, L. (2005). Conserved patterns of cell movements during vertebrate gastrulation. *Curr. Biol.* **15**, R213-R228.
Solnica-Krezel, L., Stemple, D. L., Mountcastle-Shah, E., Rangini, Z., Neuhauss, S. C., Malicki, J., Schier, A. F., Stainier, D. Y., Zwartkruis, F., Abdelilah, S. et al. (1996). Mutations affecting cell fates and cellular rearrangements during gastrulation in zebrafish. *Development* **123**, 67-80.
Strutt, D., Johnson, R., Cooper, K. and Bray, S. (2002). Asymmetric localization of frizzled and the determination of notch-dependent cell fate in the Drosophila eye. *Curr. Biol.* **12**, 813-824.
Strutt, H., Warrington, S. J. and Strutt, D. (2011). Dynamics of core planar polarity protein turnover and stable assembly into discrete membrane subdomains. *Dev. Cell* **20**, 511-525.
Tada, M. and Kai, M. (2009). Noncanonical Wnt/PCP signaling during vertebrate gastrulation. *Zebrafish* **6**, 29-40.
Teran, E., Branscomb, A. D. and Seeling, J. M. (2009). Dpr Acts as a molecular switch, inhibiting Wnt signaling when unphosphorylated, but promoting Wnt signaling when phosphorylated by casein kinase Idelta/epsilon. *PLoS ONE* **4**, e5522.
Topczewski, J., Sepich, D. S., Myers, D. C., Walker, C., Amores, A., Lele, Z., Hammerschmidt, M., Postlethwait, J. and Solnica-Krezel, L. (2001). The zebrafish glypican knypek controls cell polarity during gastrulation movements of convergent extension. *Dev. Cell* **1**, 251-264.
Tree, D. R., Shulman, J. M., Rousset, R., Scott, M. P., Gubb, D. and Axelrod, J. D. (2002). Prickle mediates feedback amplification to generate asymmetric planar cell polarity signaling. *Cell* **109**, 371-381.
Umbhauer, M., Djiane, A., Goisset, C., Penzo-Méndez, A., Riou, J. F., Boucaut, J. C. and Shi, D. L. (2000). The C-terminal cytoplasmic Lys-thr-X-X-X-Trp motif in frizzled receptors mediates Wnt/beta-catenin signalling. *EMBO J.* **19**, 4944-4954.
Usui, T., Shima, Y., Shimada, Y., Hirano, S., Burgess, R. W., Schwarz, T. L., Takeichi, M. and Uemura, T. (1999). Flamingo, a seven-pass transmembrane cadherin, regulates planar cell polarity under the control of Frizzled. *Cell* **98**, 585-595.
Villefranc, J. A., Amigo, J. and Lawson, N. D. (2007). Gateway compatible vectors for analysis of gene function in the zebrafish. *Dev. Dyn.* **236**, 3077-3087.
Wada, H. and Okamoto, H. (2009). Roles of noncanonical Wnt/PCP pathway genes in neuronal migration and neurulation in zebrafish. *Zebrafish* **6**, 3-8.
Wada, H., Iwasaki, M., Sato, T., Masai, I., Nishiwaki, Y., Tanaka, H., Sato, A., Nojima, Y. and Okamoto, H. (2005). Dual roles of zygotic and maternal Scribble1 in neural migration and convergent extension movements in zebrafish embryos. *Development* **132**, 2273-2285.
Wada, H., Tanaka, H., Nakayama, S., Iwasaki, M. and Okamoto, H. (2006). Frizzled3a and Celsr2 function in the neuroepithelium to regulate migration of facial motor neurons in the developing zebrafish hindbrain. *Development* **133**, 4749-4759.
Wallingford, J. B., Rowning, B. A., Vogeli, K. M., Rothbächer, U., Fraser, S. E. and Harland, R. M. (2000). Dishevelled controls cell polarity during Xenopus gastrulation. *Nature* **405**, 81-85.
Witzel, S., Zimyanin, V., Carreira-Barbosa, F., Tada, M. and Heisenberg, C. P. (2006). Wnt11 controls cell contact persistence by local accumulation of Frizzled 7 at the plasma membrane. *J. Cell Biol.* **175**, 791-802.
Wong, H. C., Bourdelas, A., Krauss, A., Lee, H. J., Shao, Y., Wu, D., Mlodzik, M., Shi, D. L. and Zheng, J. (2003). Direct binding of the PDZ domain of Dishevelled to a conserved internal sequence in the C-terminal region of Frizzled. *Mol. Cell* **12**, 1251-1260.
Yin, C., Kiskowski, M., Pouille, P. A., Farge, E. and Solnica-Krezel, L. (2008). Cooperation of polarized cell intercalations drives convergence and extension of presomitic mesoderm during zebrafish gastrulation. *J. Cell Biol.* **180**, 221-232.
Yin, C., Ciruna, B. and Solnica-Krezel, L. (2009). Convergence and extension movements during vertebrate gastrulation. *Curr. Top. Dev. Biol.* **89**, 163-192.
Yona, S., Lin, H. H., Siu, W. O., Gordon, S. and Stacey, M. (2008). Adhesion-GPCRs: emerging roles for novel receptors. *Trends Biochem. Sci.* **33**, 491-500.
Zeng, X. X., Wilm, T. P., Sepich, D. S. and Solnica-Krezel, L. (2007). Apelin and its receptor control heart field formation during zebrafish gastrulation. *Dev. Cell* **12**, 391-402.

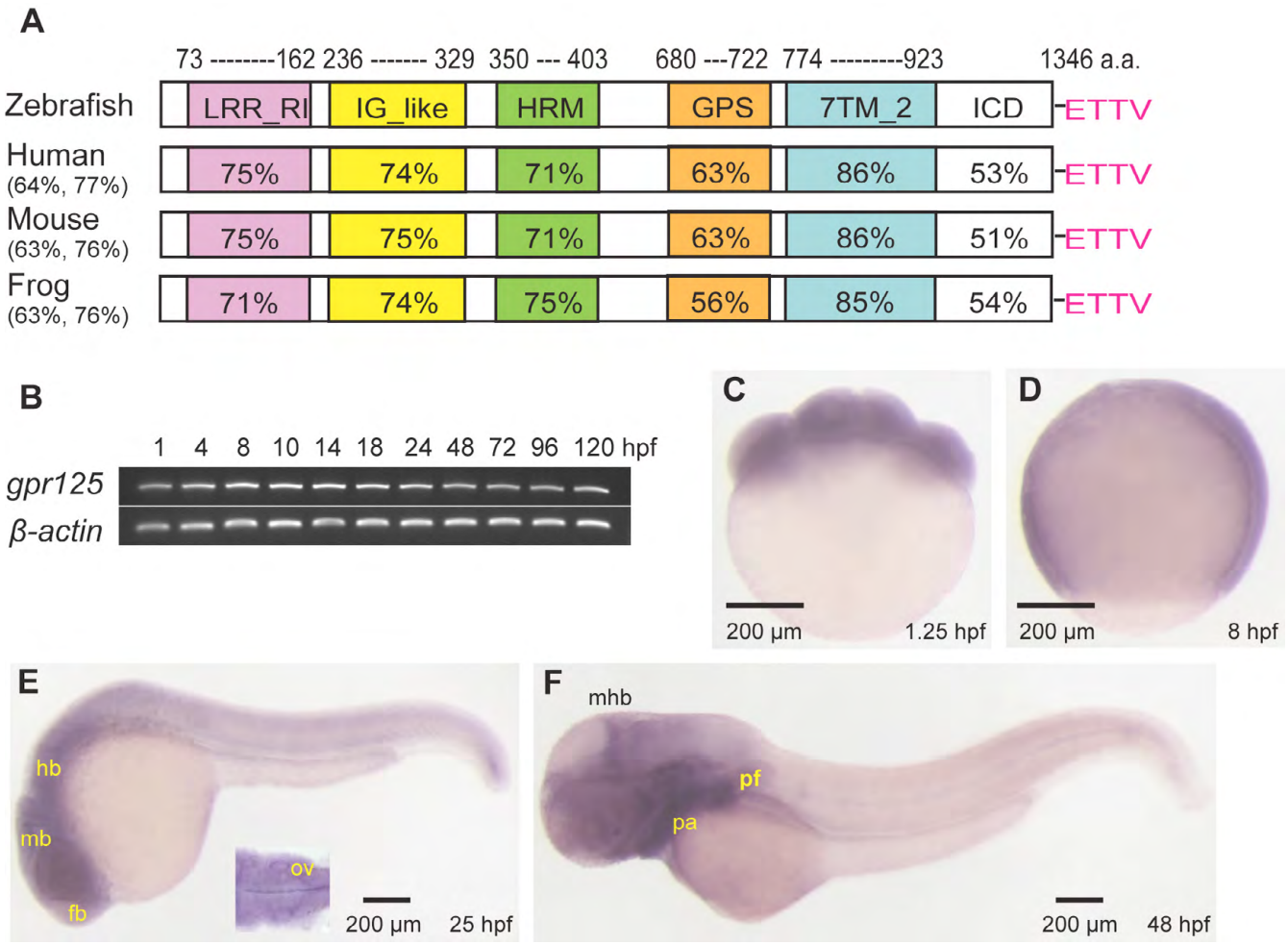

Fig. S1. Predicted protein domains and spatiotemporal expression profile of *gpr125* during early zebrafish development. (**A**) Schematics of predicted zebrafish Gpr125 protein domains. The percentage amino acid identity or similarity between Gpr125 peptide sequences in vertebrates for the whole protein are included in parentheses, and for individual domains on the schema. LRR_RI, leucine-rich repeat_ribonuclease inhibitor type; IG_like, immunoglobulin_like; HRM, hormone receptor domain; GPS, GPCR proteolytic site; 7TM_2, seven-pass transmembrane type 2; ICD, intracellular domain. The PDZ binding motif (ETTV) at the C-terminus are labeled in pink. (**B**) RT-PCR of *gpr125* transcripts from 1 to 120 hpf. β-Actin was used as a loading control. (**C-F**) Whole-mount *in situ* hybridization profile of *gpr125* expression. Lateral views, anterior is upwards in C,D and leftwards in E,F. fb, forebrain; hb, hindbrain; mb, midbrain; mhb, midbrain-hindbrain boundary; ov, otic vesicle; pa, pharyngeal arches; pf, pectoral fin.

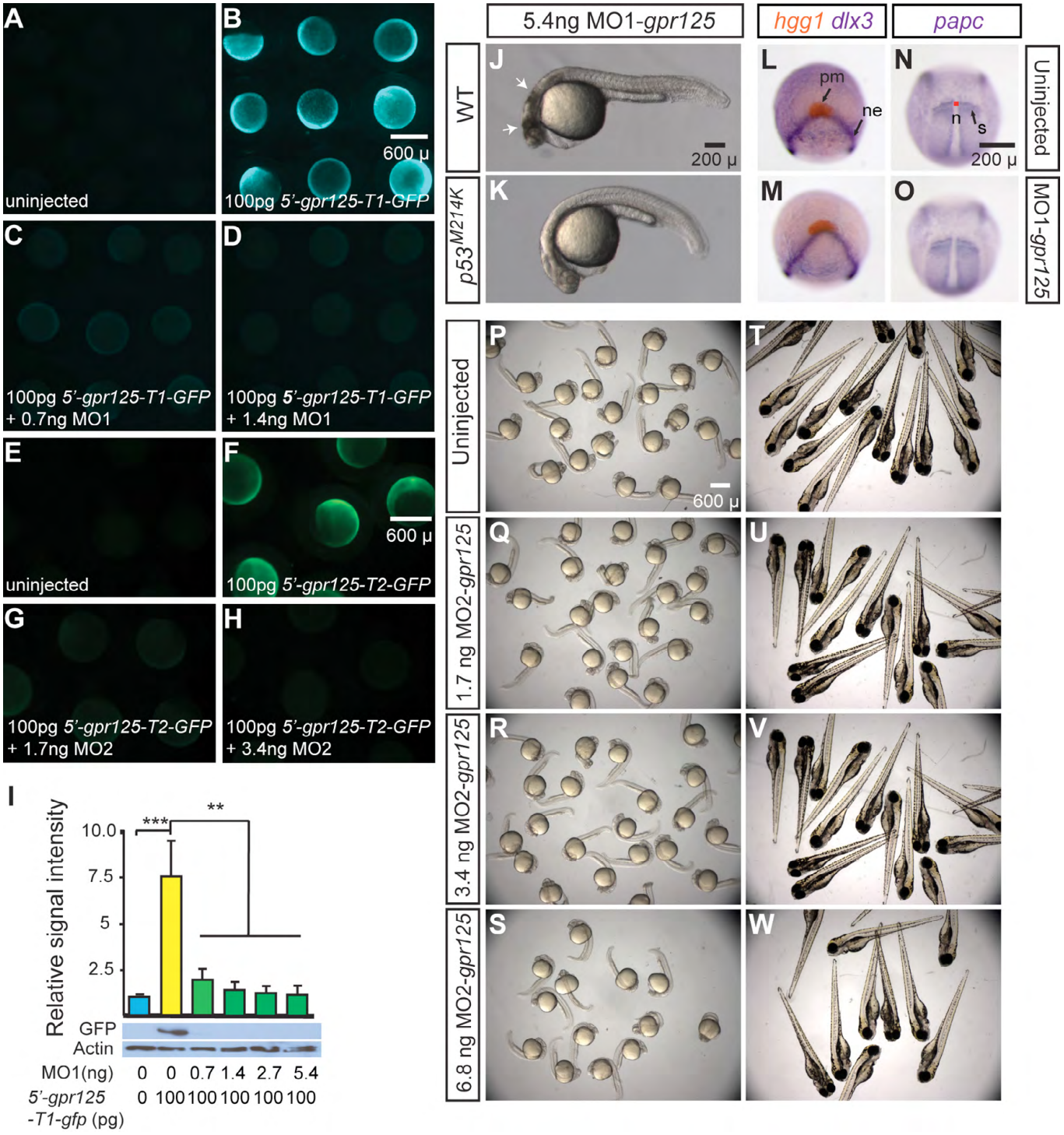

Fig. S2. Effective *gpr125* MOs cause no noticeable morphological defects in wild-type embryos. (**A-D**) Live images of uninjected (A), 100 pg *5'-gpr125-T1-GFP* RNA (GFP reporter for MO1-*gpr125*) injected (B), or 100 pg *5'-gpr125-T1-GFP* RNA and MO1-*gpr125* co-injected embryos (C,D) at the 70%-epiboly stage. (**E-H**) Live images of uninjected (E), 100 pg *5'-gpr125-T2-GFP* RNA (GFP reporter for MO2-*gpr125*) injected (F), or 100 pg *5'-gpr125-T2-GFP* RNA and MO2-*gpr125* co-injected embryos (G-H) at the 75% epiboly stage. (**I**) Western blot quantification of GFP reporter protein levels in MO1-*gpr125* injected embryos. The density of the GFP bands was normalized to that of the actin bands and the signal intensity relative to uninjected embryos is shown. Error bars indicate s.e.m. $^{**}P<0.01$, $^{***}P<0.001$. (**J**,**K**) Lateral views of 5.4 ng MO1-*gpr125*-injected wild-type (J) or $p53^{M214K/M214K}$ embryos (K) at 1 dpf. Anterior is leftwards. Arrows in J indicate regions of significant cell death. (**L-O**) Whole-mount *in situ* hybridization analyses of marker gene expression in uninjected (L,N) and 2.7 ng MO1-*gpr125*-injected embryos (M,O) at the two-somite stage. (L,M) Animal pole views, ventral is upwards. (N,O) Dorsal views, anterior is upwards. n, notochord; ne, neural ectoderm border; pm, prechordal mesoderm; s, somites. Red line in N indicates the width of the notochord at the first somites. (**P-W**) Uninjected embryos or embryos injected with increasing doses of MO2-*gpr125* at 1 dpf or 3 dpf.

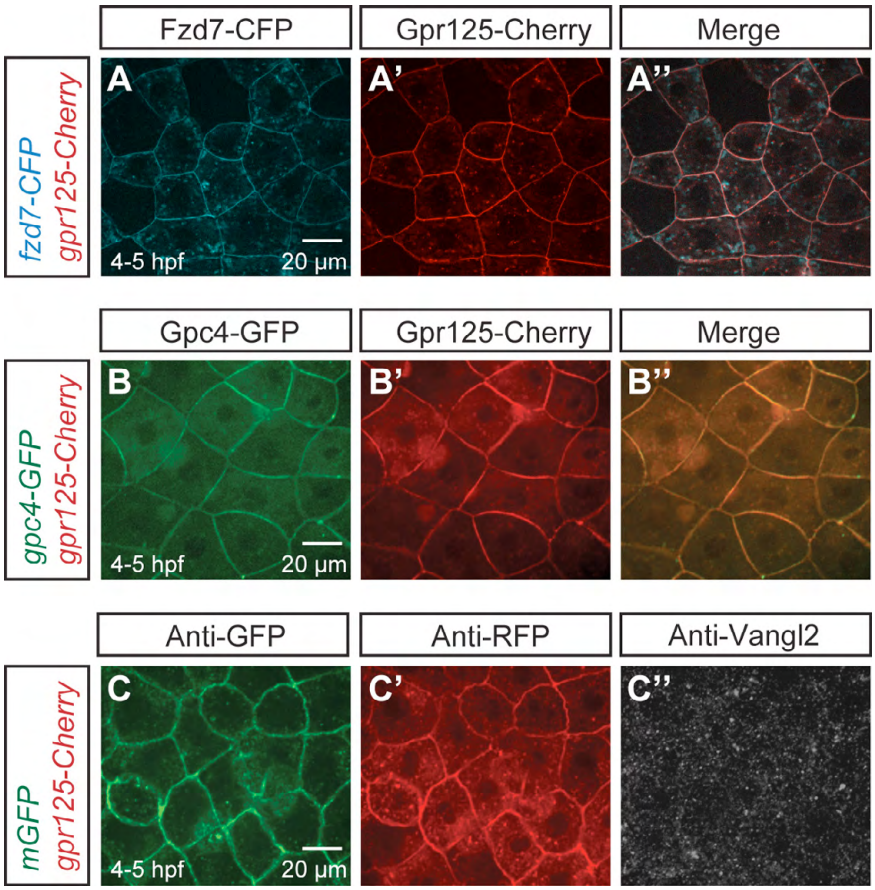

Fig. S3. Gpr125-Cherry alone did not affect PCP components localization in late blastulae (4-5 hpf). (**A-A″**) Animal pole views of a blastula co-injected with 110 pg *fzd7-CFP* and 300 pg *gpr125-Cherry* RNA. (**B-B″**) Animal pole views of a blastula co-injected with 60 pg *gpc4/kny-GFP* and 300 pg *gpr125-Cherry* RNA. (**C-C″**) Animal pole views of a 300 pg *gpr125-Cherry* and 150 pg *mGFP* RNA-injected blastula immunostained for GFP, RFP and Vangl2.

Movie 1. Gpr125-Cherry and Dvl-GFP membrane subdomains in the zebrafish blastula at 4-5 hpf.

Movie 2. Gpc4/Kny-GFP membrane subdomains in the presence of Dvl and mCherry in the zebrafish blastula at 4-5 hpf.

Table S1. Nucleotide sequences of primers and antisense morpholino oligonucleotides

Primer	**Sequence (5'-3')**
β-actin	ATGGATGAGGAAATCGCTGCCCTGGTC CCTGATGTCTGGGTCGTCCAACAATGG
gpr125-q	GGAAACTCCAGCATCCTCAG ACACGGTGGTGAAGTTGTCA
gpr125-probe	GAGCTCAAAGAACAATCCGAGGAGCA TACTCGCGCAAAACTGTGAGCCTGCTA
gpr125-probe-2	TAGGAGTGAAGGAAACTCGCTGCTCGT GCTTGACAAACGCTCGCATTGTATGTC
Cla1-5'-*gpr125*-T1-SpeI	AGAGAGATCGATTGCTAATCTGACCCCCTTCT AGAGAGACTAGTTACTCCAGCCGTCGTTGATA
Cla1-5'-*gpr125*-T2-SpeI	AGAGAGATCGATGCTCTATGGCTTTGGACGAA AGAGAGACTAGTTACTCCAGCCGTCGTTGATA
gpr125FL	ATGTCGGTGCTTTGCGTC CTACACAGTAGTTTCATGCTTCCAC
gpr125ΔETTV	GCTTGACAAACGCTCGCATTGTATGTC CTAGCTCTTCCATACCCTGCT
gpr125ΔICD	ATGTCGGTGCTTTGCGTC TCATTGTCGGTTTACGCAATGG
gpr125ΔStop codon	ATGTCGGTGCTTTGCGTC CACAGTAGTTTCATGCTTCCACA
MO	
MO1-*gpr125*	TACTCCAGCCGTCGTTGATATGTTC
MO2-*gpr125*	TAGCATATAAATAGCCTTTCCGTGC
Control MO	CCTCTTACCTCAGTTACAATTTATA

Table S2. Cyclopia indices of MO2-*gpr125* and/or *gpr125* RNA-injected *vangl2/tri*$^{vu67/vu67}$ embryos

Injection group	Cyclopia index	Number of embryos
(G1) Uninjected	2.10	63
(G1) 3.4ng MO2-*gpr125*	3.33	15
(G1) 3.4ng MO2-*gpr125* +11.5pg *gpr125*	2.83	24
(G1) 11.5pg *gpr125*	2.35	20
(G2) Uninjected	3.44	18
(G2) 3.4ng MO2-*gpr125*	4.21	19
(G2) 3.4ng MO2-*gpr125* +11.5pg *gpr125*	3.44	27
(G3) Uninjected	2.57	23
(G3) 3.4ng MO2-*gpr125*	4.00	15
(G3) 3.4ng MO2-*gpr125* +11.5pg *gpr125*	3.93	14
(G4) Uninjected	2.76	29
(G4) 3.4ng MO2-*gpr125*	3.5	24
(G4) 3.4ng MO2-*gpr125* +11.5pg *gpr125*	2.88	17
(G4) 3.4ng MO2-*gpr125* +H2O	3.62	26
(G5) Uninjected	1.59	29
(G5) 3.4ng MO2-*gpr125*	3.45	20
(G5) 3.4ng MO2-*gpr125* +25pg *gpr125*	3.28	18
(G6) Uninjected	2.39	18
(G6) 3.4ng MO2-*gpr125*	3.65	20
(G6) 3.4ng MO2-*gpr125* +25pg *gpr125*	3.35	17
(G7) Uninjected	1.75	4
(G7) 3.4ng MO2-*gpr125*	3.25	4
(G7) 3.4ng MO2-*gpr125* +11.5pg *gpr125*	2.4	5
(G7) 3.4ng MO2-*gpr125* +H2O	3.5	4
(G8) Uninjected	2.86	14
(G8) 3.4ng MO2-gpr125	3.29	7
(G8) 3.4ng MO2-gpr125 +H2O	3.75	12

G*x* denotes individual clutches of embryos.

Table S3. *gpr125* knockdown enhances the cyclopia phenotypes of *wnt11/slb*$^{tz216/tz216}$ embryos

Injection group	Cyclopia index	Number of embryos	*t*-test value
(G1) H2O	3.32	25	1.58E-04
(G1) 3.4ng MO2-*gpr125*	4.10	31	
(G2) H2O	4.10	42	4.51E-05
(G2) 3.4ng MO2-*gpr125*	4.50	40	
(G3) H2O	3.26	39	4.46E-11
(G3) 3.4ng MO2-*gpr125*	3.98	40	

G*x* denotes individual clutches of embryos.